TOWARDS NOVEL OPTICAL SENSORS

UNIVERSITY
of
GLASGOW

Graeme Smith

A thesis submitted for the degree of Master of Science

Department of Chemistry, University of Glasgow, September 2000

Acknowledgements

I would like to start by thanking my Mum, Dad and my friends for their support throughout the project, as without it none of this would be possible. I would also like to thank my supervisor Dr Andy Benniston for his sound advice and encouragement through out the duration of the project.

Thanks are also due to my colleagues in the research office for making my life at Glasgow University a little more enjoyable.

Finally, I would like to thank the EPSRC for funding.

Abbreviations

AN	Acceptor Number
bipy	2,2'-bipyridine
BUCN	Butyronitrile
d	doublet
DIBAL-H	Diisobutylaluminium hydride
dmapy	4-(dimethylamino)-pyridine
DMF	Dimethylformamide
DMSO	Dimethylsulphoxide
DN	Donor Number
EI	Electron Impact
LUMO	Lowest Unoccupied Molecular Orbital
MC540	Merocyanine 540
Me	Methyl
MHz	Megahertz
MLCT	Metal to Ligand Charge Transfer
mmol	millimoles
mol	moles
NBS	N-Bromosuccinimide
NMR	Nuclear Magnetic Resonance
ppm	parts per million
PPTS	Pyridinium toluene-*p*-sulphonate
rt	room temperature
s	singlet
SAW	Surface Acoustic Wave
SS	Stokes Shift
TACN	1,4,7-triazacyclononane
T-Bu	tert-butyl
THF	Tetrahydrofuran
TLC	Thin Layer Chromatography
UV	Ultraviolet
VIS	Visible

Structural Abbreviations

L_1

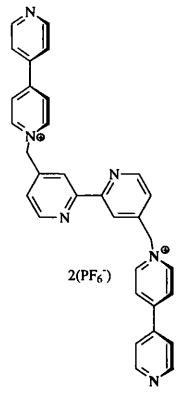

C2

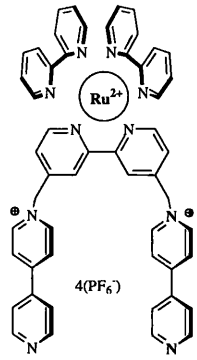

Compounds

2

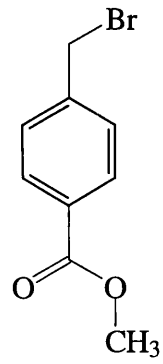

5

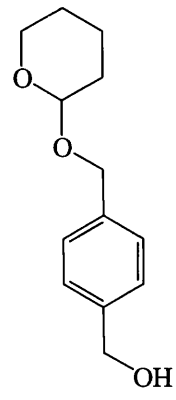

6

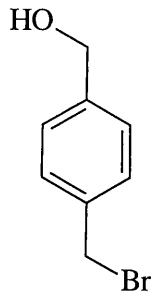

8

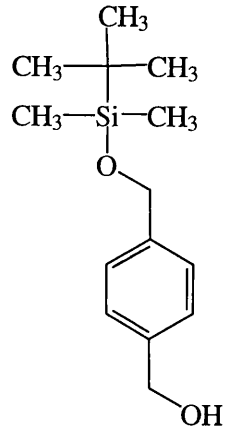

10

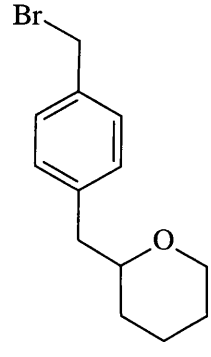

15

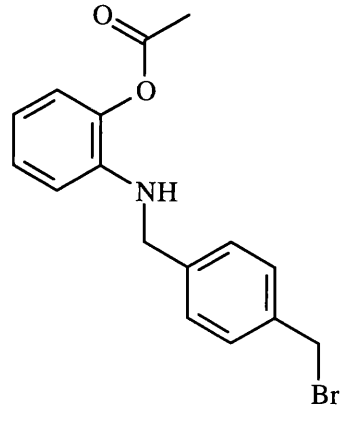

18

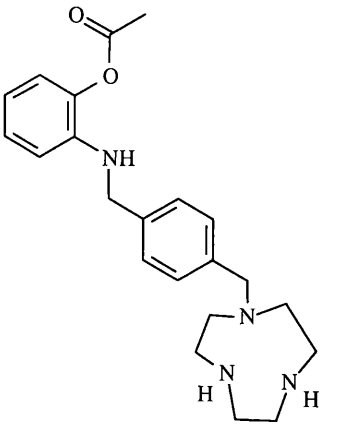

BS1

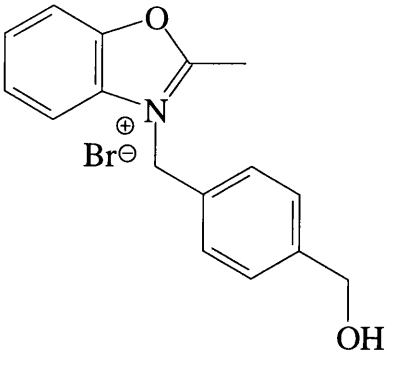

BS6

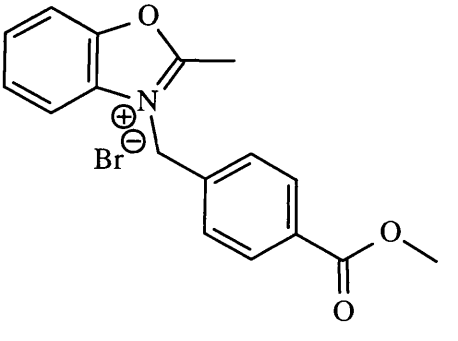

MC1

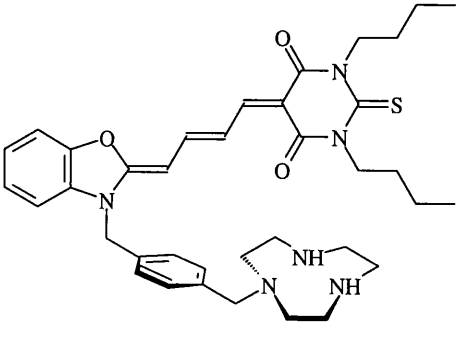

MC2

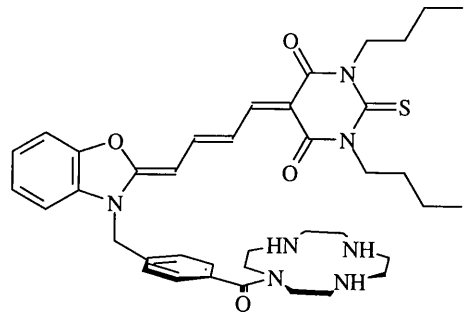

MC3

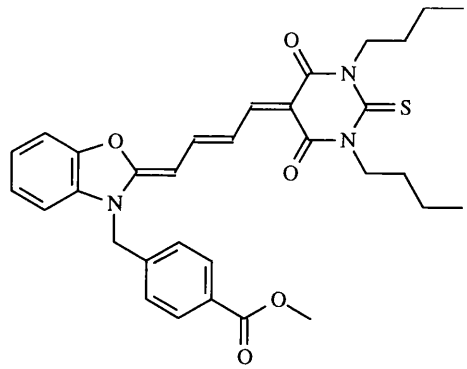

Summary

This research presented in this thesis is based in the development of optical sensors. More specifically, this project outlines two novel systems that could possible used within this field. The first system is based on a functionalized ruthenium(II) polypyridyl complex and the second is based on derivatives of merocyanine 540.

For the first system the synthesis and detailed photophysical properties of a bis(*N*-methylene-4-pyridinium-4'-pyridine) functionalized ruthenium(II) polypyridyl complex (**C2**) in solvents of varying polarity and Gutmann's donor number (DN) are discussed. The emission spectrum of (**C2**) in varying solvents was also simulated and parameters including the Huang-Rhys (S_m) obtained. Respectable correlations of the optical properties of (**C2**) with the solvent polarity factor (Δf) and DN were obtained. These results were used to calculate a difference in dipole moment between ground and excited state of *ca* 10 D, and propose a simplified potential-energy surface model to explain the results. The excited state lifetime data for (**C2**) in acetonitrile were collected over a modest temperature range of 60K. The Arrhenius plot of ln (k_{obs}) vs 1/T was found to be linear affording a proportionately low activation energy of 5.6 (± 0.2) kJ mol^{-1} when compared to the literature value of 45.5 kJ mol^{-1} for $[Ru(biby)_3]^{2+}$.

For the second system the design of novel merocyanine dyes for use in sensing and photodynamic therapy is given. The parent dye of these molecules being merocyanine 540. With its preferential uptake into leukaemia cells and their subsequent eradication by induced photosensitization, has rewarded it considerable interest over the years in the field of photodynamic therapy. Its ability to act as a photosensitizer depends greatly on its efficiency of intersystem crossing to the triplet manifold. Unfortunately

the dominant photoprocess involves photo-isomerization to form a long-lived (unstable) isomer.

It is expected that if this isomerization process could be prevented then it would lead to a much more potent photosensitizer. There have been extensive studies into the prevention of this process ranging from structural to electronic changes within the molecule, but sadly to no avail.

The design of the derivatives **MC1** and **MC2** was carried out via the incorporation of a triazamacrocycle into the structure of the molecule. It is predicted that with the binding of a metal to this macrocycle the molecule will be locked into the trans isomer and be unable to undergo photo-isomerization.

Contents

Table of Figures

CHAPTER 1

INRODUCTION: CHEMICAL SENSORS

1.1 Need for sensors

Due to the ever increasing demand for the human race to monitor all aspects of the environment around us in real time, it has become necessary to design molecules known as chemical sensors. The driving force behind which are our concerns with pollution, health and safety. With examples like the monitoring for heavy metal pollutants in natural waters or for bacteria in drinking water, swimming pool or beaches.

1.2 Chemical sensors': What are they?

Chemical sensors are molecules designed to give measured responses, resulting from chemical reactions occurring in response to a specific analyte and allowing the qualitative or quantitative analysis of that analyte.

For a sensor to work effectively it is necessary that these molecules contain two integrated or separate regions within the molecule. The first region must contain a group that is able to undergo chemical selectivity for a particular analyte and the second being the transducer. The two regions of the molecule must be able to communicate with each other for them to work.

Firstly, the selective region of the molecule must show some kind of chemical recognition for a particular molecule and give out a chemical signal, that is then amplified by the transducer region of the sensor, the magnitude of which being related to the amount of analyte present in the sample. This output can be in the form of a colour change, emission of light, change in electrical potential at a surface, a flow of electrons, the production of heat or a change in the oscillator frequency of a crystal.

1.3 Types of chemical sensors

Due to the many different forms of output that sensors possess, it has become necessary to group them together into the type of transducer present in the molecule.

i. *Electrochemical.* These include potentiometric sensors (ion-selective electrodes, ion-selective field effect transistors) and voltammetric/ amperometric sensors.

ii. *Optical.* Spectroscopic measurements are normally associated with the chemical reaction of optical sensors. Optical sensors are often referred to as 'optodes' and are frequently used in conjunction with optical fibres. The measurements used for optical sensors are generally absorbance, reflectance and luminescence.

iii. *Mass sensitive.* These make use of the piezoelectric effect and include devices such as the surface acoustic wave (SAW) sensors. The driving force behind these sensors is that of change in mass on the surface of an oscillating crystal. The degree of change in frequency caused by the change in mass being related to the amount of material absorbed on to the surface of the crystal.

iv. *Heat sensitive.* These sensors are generally known as calorimetric sensors. These sensors monitor the heat of a chemical reaction, involving the analyte, using thermistors or platinum thermometers as transducers.

The main fields within chemical sensors that have attracted the most attention are the electrochemical and optical style sensors. Both optical and potentiometric sensors have been reviewed extensively,[2,3] a review covering the comparison of the two and giving examples of each was carried out by Buhlmann *et al.*[4,5]

1.4 Electrochemical sensors

A comprehensive review by Fabry and Siebert is included in a book on solid-state electrochemistry.[6]

1.4.1 Potentiometric technique

This technique makes use of an electrical potential at the surface of a solid material that is created when the material is placed in a solution containing ions of the analyte. The resulting exchange of ions between the surface and the solution gives rise to the formation of an electrical potential, the magnitude of which is related to the number of ions in the solution.

The most common device, used for such measurements is an ion-selective electrode, these electrodes are generally classed as potentiometric chemical sensors. A review of the work by a leading scientist in this field can be found by Widmar.[7]

These sensors can under go recognition in two ways, which are referred to as direct and indirect.

i. *Direct.* The ionic guest recognition receptor creates a measurable membrane potential.

ii. *Indirect.* On recognition of the analyte the transducer region of the sensor in turn produces an ionic product that creates a measurable membrane potential.

1.4.2 Glass membrane sensor

One of the oldest and most common potentiometric sensors is the glass electrode and has been known for over 80 years. This electrode is essentially made of sodium silicate

glass, made by fusing a mixture of Al_2O_3, Na_2O, and SiO_2. This sensor gives a predominant response towards H^+ ions due to the low amount of Al_2O_3 present in the glass, for these sensors response towards other monovalent cations such as Na^+, Li^+ and K^+ can be tailored by increasing the amount Al_2O_3 present in the glass.

Before use, potentiometric chemical sensors generally have to be conditioned. For glass electrodes soaking the electrode in 0.1 M HCl for a few hours carries out this conditioning. The result of this conditioning processes is the formation of silanol groups (-SiO^-H^+) in accordance to equation 1 on the surface of the glass, and creates a hydrated gel layer on the surface of the glass that is necessary for the membrane to function.

$$—SiO^- Na^+ + H^+ \rightleftharpoons —SiO^- H^+ + Na^+ \qquad \textbf{Eq 1}$$

The silanol groups have a reversible equilibrium with the H^+ ion when the electrode is placed in aqueous solutions, a charge separation process then occurs across the glass/water interface, which results in the formation of an electrical potential difference. This difference in electrical potential is a result of the H^+ ions dissociating according to the equilibrium in equation 2. The position of this equilibrium is related to the pH of the surrounding aqueous solution that in turn determines the magnitude of the electrical potential difference across the glass/water interface.

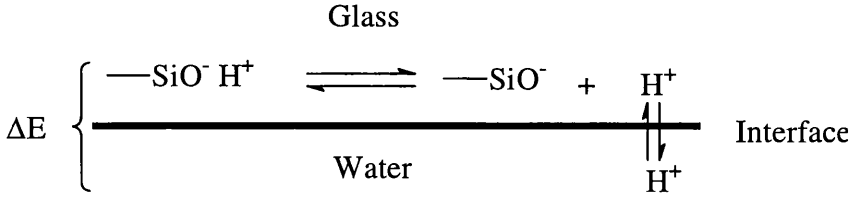

Eq 2

Experimentally the potential across the water/glass interface is measured in an electrochemical cell containing a reference electrode as shown in Figure 1.1. The potential

of the cell is given as the difference between the potential on the right hand side and the left hand side of the cell (equation 3).

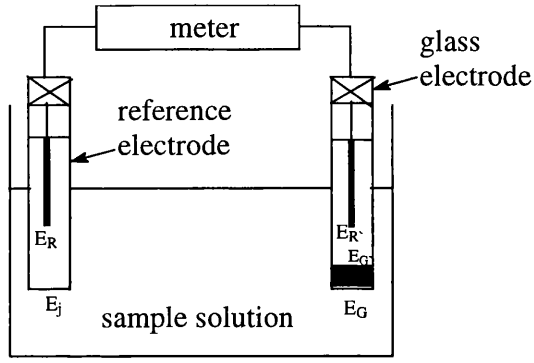

Figure 1.1 Example of an electrochemical cell.

$$E = E_G + E_{G`} + E_{R`} - E_R - E_J \qquad \textbf{Eq 3}$$

Where E_G and $E_{G`}$ are the potentials of the two glass/water interfaces, $E_R$ and $E_{R`}$ the two reference element potentials and the E_J liquid junction potential. In the above cell it is assumed that all the potentials remain constant apart from the E_G value which represents the pH of the solution.

The cell potential is given by the Nernst equation in the following form, equation 4.

$$E = \text{constant} + RT/nF \ln a_{H^+_{aq}} \qquad \textbf{Eq 4}$$

The equation can then be simplified to the form shown in equation 5.

$$E = \text{constant} - 59.1\ \text{pH} \qquad \textbf{Eq 5}$$

The constant being the interface potentials, pH equaling $-\log_{10} a_{H+}$ and 2.303 RT/nF is equal to +59.1 at 25 °C. Now when the potential across the water/glass interface is measured the pH of the solution can be calculated and then in turn the concentration of H^+ ions in the solution. This shows how the glass electrode can be used for the sensing of H^+ ions.

1.4.3 Advantages and disadvantages of the electronic transducer

The advantages of sensors with this type of transducer are that they have a very large working concentration range and generally robust and reusable. However, they also have their disadvantages since they are subject to interference from other electronic species and will pick up background noise from the instrumentation being used. The length of wire used to connect the sensor to the amplifier/ recorder also limits their use. Also with increased lengths of wire the amount of background noise picked up will increase. The final disadvantage with this type of transducer is they require a separate reference electrode to complete the electrical cell.

1.5 Optical sensors

An optical sensor relies on the presence of an optical transducer and has spawned from classical ultra-violet/visible (UV/Vis) spectroscopy. Classically this form of spectroscopy involves placing a solution of the analyte into the path of a well-defined incident beam of light, and then the collection of the radiation that is transmitted. The intensity of which can then be related to the concentration of the analyte through the Beer Lambert law equation 6.

$$A = \varepsilon \, . \, l \, . \, [M] \qquad \textbf{Eq 6}$$

Where A is the absorbance, ε is the molar absorptivity ($mol^{-1}Lcm^{-1}$), l is the path length (cm) and [M] is the concentration (mol/L).

In most case a reagent or reagents have to be added to the analyte to produce the coloured species that absorbs light at the wavelength of the incident light. However, this

conventional form of UV/Vis spectroscopy involves a homogeneous solution containing the reagents and the analyte.

For most cases of optical sensors a two-phase system is incorporated with the reagent responsible for the colour change being immobilized in or on a solid substrate or within a membrane attached to a solid substance. Then when the substance comes in contact with the analyte in solution a colour change occurs. This type of material is known as an 'optode' analogous to the term 'electrode'.

This process of binding or absorbing the reagent onto the surface of glass or plastic, or immobilizing them into a membrane is ideal for coupling with optical fibres. This coupling of the immobilized reagent and optical fibres gives rise to very versatile sensors that can be used for remote sensing. [8-11]

1.5.1 Optical fibres

Similar to electrical transducers a medium for carrying the signal to and from the sensor is needed. For electrical sensors the wires connecting the sensor to the amplifier carry out this function. In optical sensors the medium used is optical fibres (Figure 1.2). Optical fibres are made of three sections which are the core, cladding and an outside coating. The core of the fibre is made of silica,

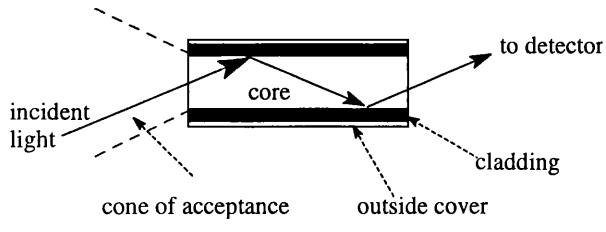

Figure 1.2 Pictorial representation of an optical fibre depicting the reflectance of light down the core.

plastic or glass and then surrounded by an optical insulator (cladding). An outside cover then protects these layers. It is essential that the refractive index of the cladding is lower than that of the core in order for the light to be reflected down the core.

These fibres work by light entering one end of the core, within the cone of acceptance, the light is then reflected down the core of the fibre towards the other end. These fibres are ideal for remote sensing as they can transmit light over large distances and as they can be bent through slight angles they can be incorporated into a wide range of optical sensing devices.

1.5.2 Absorbance techniques

The simplest technique used when coupling the sensor with an optical fibre is to use the optical fibre extrinsically, to solely transport light to and from a solution of the analyte. The solution must already be in a form that is able to absorb radiation or have already been treated with a reagent. Similar to conventional UV / Vis spectroscopy the analyte solution must be in a cuvette or flow cell.

Another technique is to use the optical fibre intrinsically, which is normally employed if a reagent is needed to produce a colour change. The reagent or reagents are immobilized in a plastic film or chemically bound to the optical window of the fibre. In this technique light is

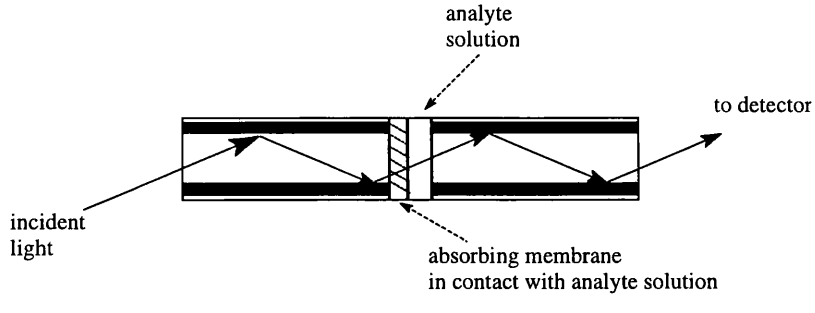

Figure 1.3 Use of optical fibre intrinsically for the measuring of absorbance.

passed down the fibre and then through the bound reagent which is in direct contact with the analyte solution. The transmitted light is then collected by a second fibre which carries the light back to the spectrometer were the signal is analysed and the intensity of the colour related to the concentration of analyte. This process is depicted in Figure 1.3.

1.5.3 **Reflectance technique**

In some cases the optodes membrane is opaque, and so light will not be transmitted through the optical window. However the optode can still interact with the analyte to give a colour change. In this case the light reflected back off the window can be collected and analysed. By careful calibration the concentration of the analyte can still be determined. Calibration is needed as the intensity of the light reflected and the concentration of the analyte are non-linear. Here the same optical fibre is used to send the light to and from the sample as shown in Figure 1.4.

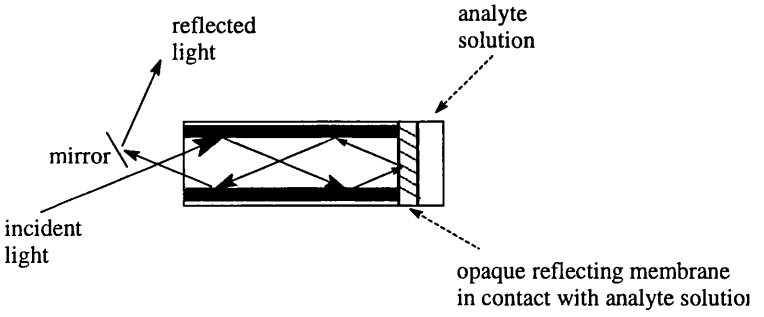

Figure 1.4 Pictorial representation of the reflectance technique.

1.5.4 Luminescence

Luminescence is probably the oldest and most established analytical technique and still used today. It has been established that there are two forms of luminescence-fluorescence and phosphorescence. The first documented record of this process was by the Spanish botanist Nicolas Monardes in 1565. He observed fluorescence from an aqueous

extract of Lignium Nephiticium. It was not until another 280 years that John Herschel recorded the first crude emission spectrum in 1845 from quinine. Then in 1852 George Stokes was the first to determine that the fluorescence emission spectrum occurred at higher wavelength than the excitation wavelength. He also found that the intensity of the fluorescence could be quenched by itself, and by other non-fluorescent molecules. From this he concluded that fluorescence could be used for the detection of organic substances. Goppelsroder was then the first to use fluorescence as an analytical tool in 1867 in the analysis of aluminium (III) ions.

Luminescence occurs when an electronically excited molecule undergoes a radiative transition to give an emission of radiation. Before the excitation of a molecule it is present in the ground state (normally the S_0 state), to which it will return in some way after excitation. On excitation, the molecule will enter into a vibrationally excited form of the S_1 state and from here it can do two things. First it can undergo radiative decay to produce luminescence, or it may undergo non-radiative decay, which involves the expulsion of energy in some way other than light. This is typically in the form of heat.

If the molecule undergoes radative decay there are two possible pathways that it can take.

(a) The molecule can emit radiation and the molecule will relax from the S_1 state to the ground state S_0 which both have the same spin multiplicity. This process is called fluorescence.

(b) Intersystem crossing to the triplet manifold can occur which involves a change in the spin multiplicity. Now when the molecule emits radiation it is relaxing from the T_1 state to the ground state S_0. This process is called phosphorescence.

Process A is spin allowed whereas process B is spin forbidden. Because of this fluorescence and phosphorescence occur on different time-scales. The lifetime of fluorescence is short between 10^{-7} to 10^{-10} seconds, whereas phosphorescence has a longer lifetime of between 10^{-3} to 10 seconds. These processes are shown in the Jablonski diagram (Figure 1.5) below.

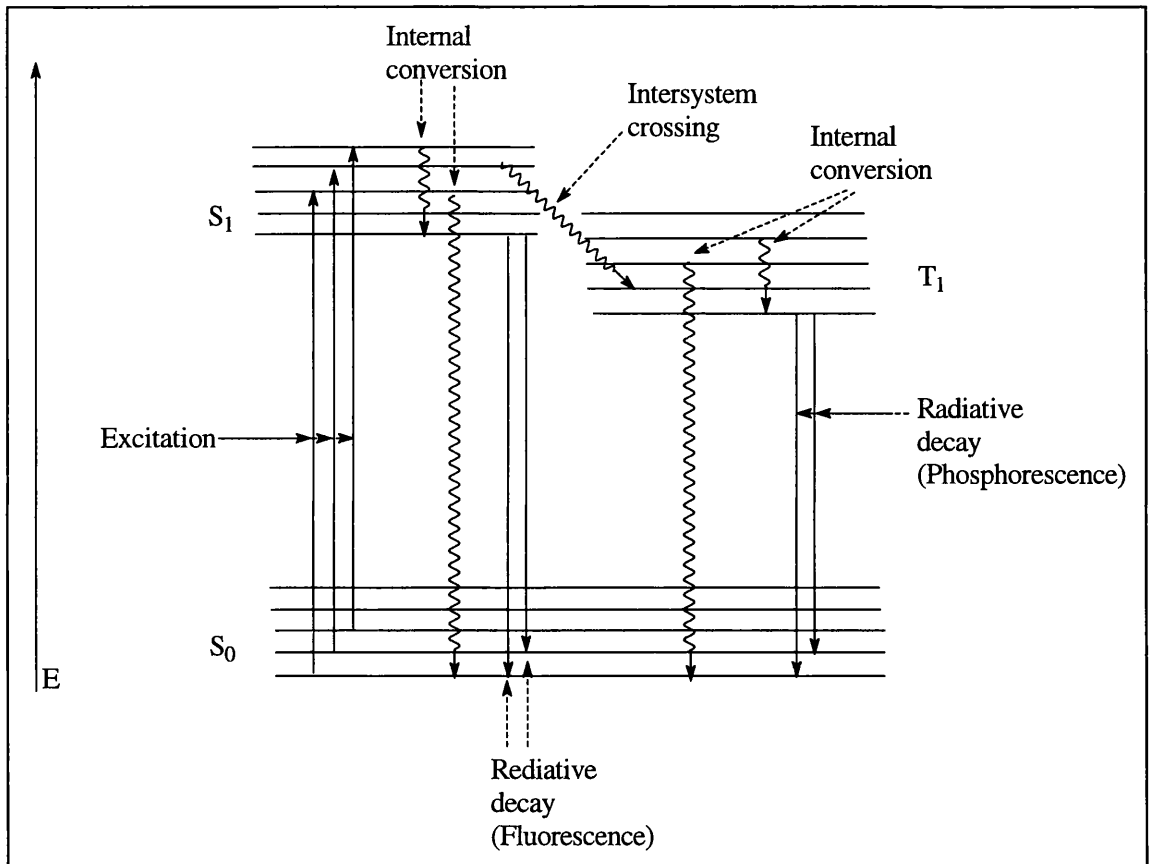

Figure 1.5 Schematic electronic state energy level diagram, describing the processes of fluorescence and phosphorescence.

In the field of optical transducers fluorescence is thought to be the optimal transduction mechanism especially for biological systems. Here are some of the advantages offered by fluorescence.

a) Fluorescence is easily and sensitively detected. Fluorescence allows for the detection of analytes that are at very low concentration, and even has the ability to detect single molecules. As the excitation and emission wavelengths are different it is possible to read the emission signal against an essentially zero background. Therefore only a low concentration of sensor is needed.

b) As fluorescence is a molecular phenomenon it allows for very good resolution when used within microenvironments. As a result of this it is possible to use these sensors within cells and still receive well-resolved signals.

c) Fluorescence is non-destructive, in other words these sensors will be able to enter cells and sense for an analyte without the destruction of the host environment.

d) Monitoring both the excitation and emission spectra allows for increased analytical sensitivity, as the emission can be monitored in three ways; intensity, intensity ratio and lifetime measurements, as well as monitoring the absorbance spectra.

e) As fluorescence has an excited state lifetime of around 10^{-7} to 10^{-10} seconds it allows for the possibility of real time assays.

f) With the immobilization of the sensor onto an optical fibre it allows for robust probes. However this will remove their capacity to infiltrate cells and to sense within microenvironments.

As well as possessing these advantages there are several difficulties encountered with the use of fluorescent sensors.

a) Measuring two different experimental variables, excitation and emission will result in it being a more expensive process than the likes of absorbance transuding.

b) Other quenchers or impurities within the sample can distort the fluorescent signal.

c) Within biological systems there will be distorting background fluorescence from the presence of protein residues that fluoresce as well.

d) Fluorescent chemosensors will undergo auto quenching and distortion of the emission spectrum at higher concentrations. This results in a limited working concentration in comparison to electrochemical systems.

1.5.5 Fluorescence techniques

There are many ways the fluorescent signal can be effected by the presence of an analyte and they can be placed into the following category: intensity, intensity ratio and lifetime measurements.

INTENSITY MEASUREMENTS

Intensity measurements are the most common form of fluorescence transuding used today. Detection is based on the complexation of an analyte to the free sensor. In these measurements the emission spectra of the free unbound sensor is directly compared to that of the bound spectra. The binding of the analyte should result in the increase or the decrease in the intensity of fluorescence at a single wavelength of the emission spectra. If there is an increase in the fluorescence it is called chelation-enhanced fluorescence and a

decrease is called chelation-enhanced quenching in the intensity. The resulting increase or decrease is proportional to the concentration of the analyte and follows the following expression (equation 7).

$$I_f = 2.303 \cdot \phi_f \cdot I_0 \cdot \varepsilon \cdot l \cdot [M] \qquad \textbf{Eq 7}$$

Where ϕ_f is the fraction of total no. of photons absorbed those results in fluorescence emission, I_0 = intensity of excitation radiation, ε is the molar absorptivity and l is the path length.

A more rigorous form of intensity measurements is that of intramolecular photoelectron transfer, resulting in the possibility of an on/ off switch within the molecule. This is possible by the incorporation of a ligating/ quenching unit within the molecule that is a set distance from the fluorophore.

This ligator/ quencher quenches the fluorescence from the flourophore resulting in no fluorescence being emitted by the free unbound molecular sensor. Upon the binding of the analyte the quenching process is prevented and results in fluorescence from the fluorophore. The intensity to which it fluoresces is directly related to the concentration of the analyte within the sample. The design and use of these types of sensor is outlined by De Silva[12-13] and others.[14]

INTENSITY RATIO MEASUREMENTS

Intensity ratio measurements are achieved via monitoring multiple excitation/ emission wavelengths, for the decrease of signal intensity of the free unbound sensor and the emergence or increase of a new signal in a different area of the spectra.

One way in which this mechanism is obtained involves excimers. Excimer formation results by increasing the concentration of the fluorophore and results in the formation of a new emission signal that is red-shifted in respect to the unbound flourophore. This shift towards the red is a result of an energy transfer from one flourophore to that of the ground state of the same or different species.

The ratio that is formed between the monomer and the excimer fluorescence intensity is governed by the flexibility of the spacer between the two chromophores. With the binding of the analyte this distance between the two chromophores will drastically change and result in the formation of a new emission.

The use of this type of sensor can be found by the conformation effect of linked anthracene excimers discussed by Ferguson *et al.*[15] and is used by Bous-Laurent *et al.*[16] for spacial and metal recognition studies.

LIFETIME MEASUREMENTS

The advantage of this type of measurement is the exact sensor concentration is not needed and therefore removes the variables such as photo-bleaching, dispersal and washout. Lifetime measurements are based on the increase or decrease of the lifetime of fluorescence resulting from the binding of an analyte to the molecular sensor. This change in lifetime can be related to the concentration of the analyte by the following expression (equation 8).

$$\tau_0/\tau = 1 + K_{sv}\,[A] \qquad \textbf{Eq 8}$$

Where τ_0 is the original lifetime and K_{sv} is the lifetime constant for the sensor.

These three methods of fluorescence measurement show how these types of sensors can give increased analytical sensitivity for use in molecular sensing.

1.6 Examples of optical sensors

By combining a flourogenic unit with a cation-selective binding site gives rise to sensor capable of sensing for particular metal cations. The main interest in this field is for the monitoring of trace amounts of essential metal cations in biological material such as blood and tissue.[17,18]

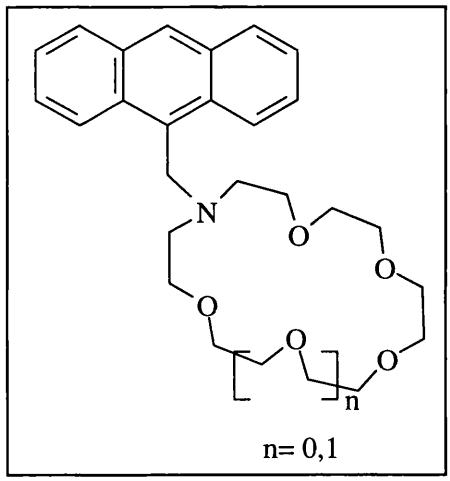

De Silva *et al.* have reported the synthesis and properties of N-(9-anthrylmethyl)monoaza-18-crown-6.[19] In this system it was found that the electron pair located on the nitrogen atom quenches the fluorescence from the anthracene unit via electron transfer. Then upon complexation with an alkali cation the fluorescence is then again observed, as the electrons responsible for the quenching are redirected towards the cation. It was found that by the addition of sodium and potassium ions the fluorescence was enhanced by a factor of *ca.* 47, all other parameters such as absorbance and emission remained the same. This system was not effected by the presence of lithium cations and can therefore be regarded as a sensor for sodium and potassium ions.

A similar system using fluorogenic crown ethers was designed by Valeur and co-workers, which used 7-dimethylamino-3-(p-formylstyrl)-1,4-benzoxazin-2-one as the

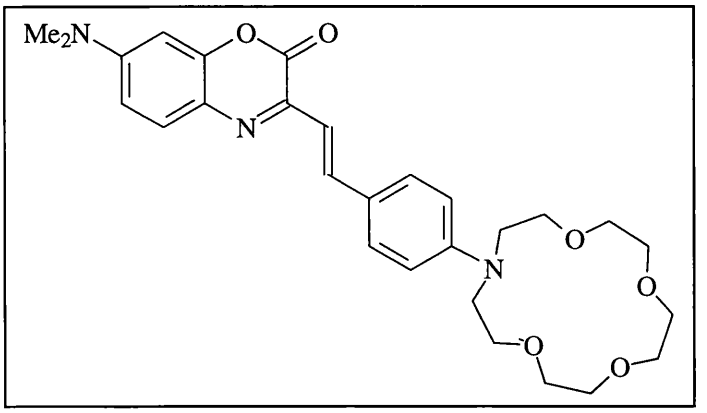

fluorescence unit coupled with a monoaza-15-crown-5 as the binding site.[20] This system was found to undergo a substantial shift in the wavelength of emission to a shorter wavelength with the addition of alkaline earth metal cations. The largest shift was observed for the addition of calcium cations. Spectral characteristics as well as stability constants for the binding of alkaline earth metal cations with the crown ether were also reported for this sensor.[21]

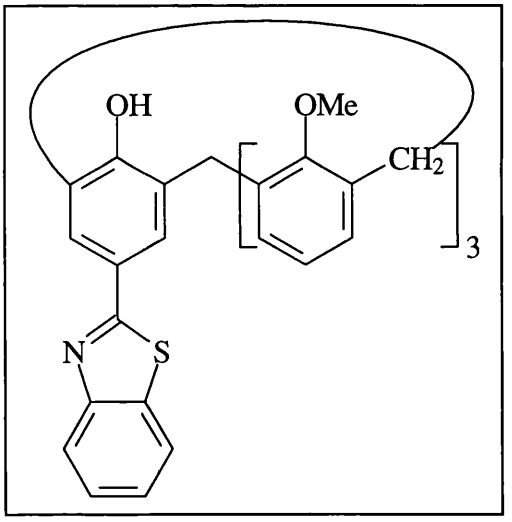

Another important binding group in sensor design is the calixarenes. Shinkai and co-workers introduced benzothiazole as a fluorophore into the structure of calix{4}-arene.[22] The result of which was a shift in the maxima of both the absorption and emission spectra but only in the case of lithium salts. Predominantly allowing its use for the detection for lithium ions.

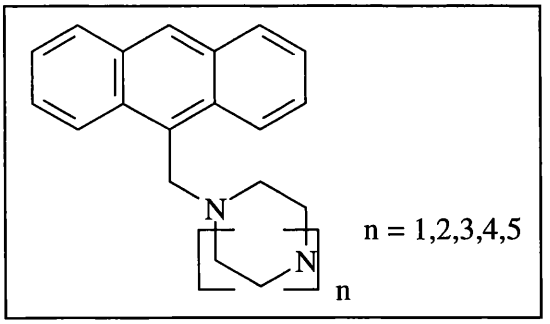

In order to sense for transition metals Czarnik and co-workers synthesized fluorescent polyamines by linking a range of polyazamacrocycles to a 9-anthrylmethyl unit.[23] Water solutions of these systems

underwent fluorescence enhancement with cadmium (II) and zinc (II), while undergoing fluorescence quenching in the presence of mercury (II) ions.

A similar system using tetraazadioxa-18-crown-6 have also been synthesized by Czarnik and co-workers and includes fluorescence titrations with Zn^{II}, Ca^{II}, Na^{I}, Ni^{II}, Co^{II} and Pb^{II} ions.[24] Czarnik has also published an overview of fluorescent chemosensors.[25]

References

1: Cattrall R. W., *Chemical Sensors*, Oxford University Press Inc., New York, 1997.

2: DeVaney D. M., Janata J., Josowicz M., Vanysek P., *Anal. Chem.* **1998**, 70, 179.

3: Hill H. H., Lopez-Avila V., *Anal. Chem.*, **1997**, 69, 289.

4: Bakker E., Buhlmann P., Pretsch E., *Chem. Rev.*, **1997**, 97, 3063.

5: Bakker E., Buhlmann, Pretsch E., *Chem. Rev.*, **1998**, 98, 1593.

6: Fabry P., Siebert E., Electrochemical sensors. In *The CRC Handbook of Solid State Electrchemistry*, Bouwmeester H. J. M.,Gellings P. J., Eds, CRC, Baco Raton, 1997, pp 329-369.

7: Widmer H. M., *Anal. Methods Instrum.* **1993**, 24(1),60.

8: Boisde G. E., Harmer A., Eds., *Chemical and Biochemical Sensing with Optical Fibers and Waveguides*, Artech House, Norwood, MA, 1996.

9: Blum L. J., Ed., *Bio- and Chemi-Luminescent Sensors*, World Sci, Singapore, 1997.

10: Griffiths P. R., Lewis I. R., *Appl. Spectrosc.* **1996**, 50 (10), 12A.

11: Udd E., *Rev. Sci. Instrum*, **1995**, 66 (8), 4015.

12: Bryan A. J., De Silva A. P., De Silva S. A., Rupasinghe R. A. D. D., Sandanayake S., *Biosensors*, **1989**, 4, 169.

13: Bissell R. A., De Silva A. P., Gunaratne H. Q., Lynch M. P. L., Maquire G. E. M., Sandanayake S., *Chem. Soc. Rev.*,**1992**, 187.

14: Czarnik A. W., *Acc. Chem. Res.*, **1994**, 27, 302.

15: Ferguson J., Morita M., Puza M., *Chem. Phys. Lett.*, **1976**, 42, 288.

16: Bous-Laurent H., Desvergne J. P., Fages F., Marsau P., *Pure and Appl. Chem.*, **1992**, 64, 1231.

17: Hoelz D. F., Steck T. L., Wallack L., *Anal. Chem.*, **1963**, 35, 1035.

18: Rink T. J., *Pure Appl. Chem.*, **1983**, 55, 1977.

19: De Silva A. P., De Silva S. A., *J. Chem. Soc. Chem. Commun.*, **1986**, 1709.

20: Fery-Forgues S., Guette J. P., Le Bris M. T., Valeur B., *J. Chem. Soc. Chem. Commun.*, **1988**, 384.

21: Fery-Forgues S., Guette J. P., Le Bris M. T., Valeur B., *J. Phys. Chem.*, **1988**, 92, 6233.

22: Araki K., Fujishima H., Iwamoto K., Shinkai S., *J. Chem. Soc. Perkin Trans. 1,* **1992**, 1985.

23: Akkaya E. U., Czarnik A. W., Huston M. E., *J. Am. Chem. Soc.*, **1990**, 112, 3590.

24: Chae M. Y., Cherian X. M., Czarnik A. W., *J. Org. Chem.*, **1993**, 58, 5797.

25: Czarnik A. W., Ed, *Fluorescent Chemosensors for Ion and Molecular Recognition*, American Chemical Society, Washington DC, 1993.

Chapter 2

Experimental

2.1 Instrumentation

2.1.1 NMR Spectroscopy

NMR spectra were obtained on a Bruker AM360 360 MHz FT-NMR spectrometer using the Bruker Aspect 3000 suite of programs. Two dimensional spectra were obtained on a Bruker DPX 400 MHz NMR spectrometer using the *en-suite* of programs. All samples were referenced internally to solvent resonances. Deuterated solvents were used as purchased.

2.1.2 Mass Spectroscopy

Mass spectra were obtained using a JEOL JMS 700 ("The MStation") mass spectrometer.

2.1.3 UV-VIS Spectroscopy

Electronic spectra were obtained using a Shimadzu UV-3101 PC spectrometer. Reference and sample spectra were collected using optically matched 1cm quartz cuvettes. Corrected spectra were produced by sample-reference subtraction using the *en-suite* of programs.

2.1.4 Fluorescence Spectroscopy

Steady-state fully corrected fluorescence spectra were obtained on a Fluoromax-2 spectrofluorimeter using the *en-suite* of programs. Spectra were obtained in 1cm quartz cuvettes.

2.1.5 Nanosecond laser Spectroscopy

Measurements were performed using a Spectron Laser Services SL803 Q-switched Nd YAG solid state laser operating at 532nm. The laser pulse duration was 15 ns at an output energy of 800μJ. Laser energy was monitored using a Laser Precision Corporation RM-6600 universal radiometer. Transient fluorescence spectra were recorded using an Applied Photophysics photomultiplier, an Applied Photophysics F/3.4 monochromator and a Tektronix TDS520 two channel digitising oscilloscope. All data was analysed using an On Line Instrument Systems kinetic fit (1989) program. Lifetime values were found to be independent of monitoring wavelength.

2.1.6 Emission Band-shape Analysis

Performed using an adaptation of the method reported by Harriman and co-workers.[1] Mathematical calculations were performed using the commercial package MATHCAD and processed in a commercial spreadsheet in which simulated and observed spectra were fitted.

2.7 Fluorescence Quantum Yield

Quantum yield of fluorescence was calculated by measuring emission intensity over a range of laser powers for optically matched samples of (2) and $[Ru(bipy)_3]^{2+}$ as standard (std) (Φ = 0.062), and using the equation: where $\frac{\phi(2)}{\phi std} = \frac{m(std)}{m(2)}$ m = slope of signal intensity *vs* laser power.

2.1.8 Molecular Modelling

Molecular modelling calculations were carried out using Hyperchem (release 4.5 for windows, © Hypercube Inc. 1994) molecular modelling and simulation software. Geometry optimisations of the molecular models were carried out using the MM+ force field, utilising a Block-diagonal Newton-Raphson algorithm, terminating at a gradient of 0.002 kcal/Åmol.

2.2 Materials and Solvents

Chemicals, their suppliers and purity used in the synthetic work are listed in table 2.2.1. Solvents and purifacation methods are listed in table 2.2.2.

Table 2.2.1 Chemicals and suppliers

Acetic Acid	Fisher	99%
Aluminium Chloride	Aldrich	97%+
2-Aminophenol	Aldrich	99%
Ammonium hexafluorophosphate	Aldrich	95%
2,2`-Azobis-2-methylpropionitrile	Jenssen	98%
Benzaldyhde	Fisons	99%
4-(Bromomethyl)-benzonitrile	Aldrich	99%
Calcium carbonate	BDH	99%
1,3-Dihydropyran	Lancaster	97%
Diisobutylaluminium hydride in toluene	Aldrich	25%wt%
Hydrobromic acid	Aldrich	48%
Hydrochloric acid	Rhedel	37%

Imidazole	Aldrich	99%
Lithium aluminium hydride	Aldrich	95%
Magnesium sulphate	Aldrich	99%
2-Methyl benzoxazole	Aldrich	99%
4-Methylcatechol	Aldrich	98%+
Methyl-4-methylbenzoate	Aldrich	99%+
N-bromosuccinimide	Aldrich	99%
Phosphorus tribromide	Aldrich	99%
Pyridinium toluene-*p*-sulphonate	--------	-----
Sodium borohydride	Koch Light	98%
Sodium hydrogen carbonate	Fisher	99%
Sodium hydrogen sulphate	Aldrich	----
Sodium Hydroxide	Aldrich	97%+
Tert-butydimethylsilylchloride	Aldrich	96%
Triethylamine	Lancaster	99%
Trimethylsilylbromide	Aldrich	97%
Triphenylphosphine	Hopkin + Williams	----

Table 2.2.2 Solvents and purification methods

Acetonitrile	Distilled from calcium hydride under N_2.
Carbontetrachloride	Distilled from phosphorus pentoxide under N_2.
Diethyl ether	Distilled from sodium wire, Benzophenone under N_2.
Dimethyl formamide	Distilled under vacuum and then stored over 4Å sieves.

40-60°C Petrolium ether	Distilled from sodium wire under N_2.
Tetrahydrofuran	Distilled from sodium, benzophenone under N_2.
Toluene	Distilled from sodiun, benzophenone under N_2.

All other solvents used were of technical grade and used without further purification.

2.3 Synthesis

2.3.1 4,4`-Bipyridinium Functionalized Ruthenium (II) Polypyridyl Complex

The ligand $\mathbf{L_1}$ and $Ru(bipy)_2\mathbf{L_1}](PF_6)_2$ (**2**) were prepared according to the literature.[2,3]

2.3.2 Novel Merocyanine Derivatives

2.3.2.1 Reaction Scheme 1

1. Bromomethyl 4-methyl benzoate (2)

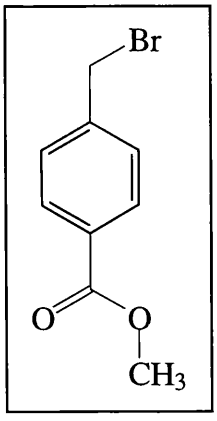

Compound **2** was prepared using the method of Bayle-Lacoste and co-workers.[4] A solution of methyl 4-methyl benzoate (30.09g, 0.2 mol) in carbontetrachloride was magnetically stirred while n-bromosuccinimide (41.08g, 0.23mol) was added portion wise. Next 2,2`-Azobis-2-methylpropionitrile (111mg) was added and the solution was illuminated with a 200W lamp, brought to reflux under N_2 and left for 4 hours. The mixture was then filtered and the excess solvent removed via

vacuum to give a white solid. The product was identical by ^{1}H NMR spectroscopy (360 MHz) with the data reported.

Yield = 46g (99.9%)

^{1}H NMR (360 MHz $CDCl_3$): δ = 3.8 ppm (s, 3H, CH_3-O), 4.4 ppm (s, 2H, CH_2-Br), 7.25-7.95 ppm (m, 4H, aromatic protons)

2. Hydroxymethyl 4-methyl benzoate (3)

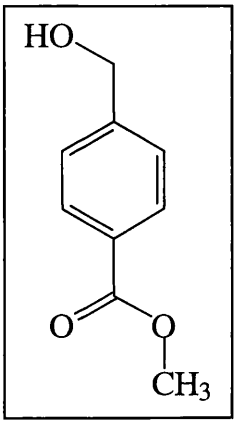

To a solution of **2** (46g, 0.2mol) in p-dioxane (500ml) was added a solution of calcium carbonate (92g) in water (500ml). The mixture was magnetically stirred and left refluxing overnight, after which any excess calcium carbonate was filtered off. The product was then extracted into dichloromethane and the organic layers collected and dried over magnesium sulphate. The solvent was then removed under vacuum to give yellow/white solid. The impure product was then recrystallised from a toluene/ petrol mixture.

Yield = 12.14g (36%).

^{1}H NMR (360 MHz $CDCl_3$): δ = 3.89 ppm (s, 3H, CH_3-O), 4.75 ppm (s, 2H, CH_2-OH), 7.40-7.42 ppm (d, 2H, atomatic protons), 7.9-8.0 ppm (d, 2H, aromatic protons).

3. 4-(Tert-butyl-dimethyl-silanyloxymethyl)-benzoicacid methyl ester (7)

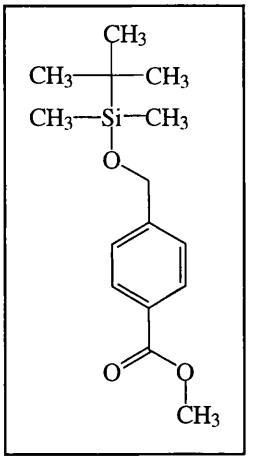

Compound **7** was prepared using the method outlined in Vogel.[5] To a solution of **3** (6g, 0.036 mol) and tert-butydimethylsiliyl chloride (5.67g, 0.0378mol) in dry DMF (20 ml) was added imidazole (5.02g, 0.072mol). The solution was then left stirring overnight and the product extracted into petrol. The organic layers were washed with saturated sodium hydrogen carbonate solution and dried over magnesium sulphate, the solvent was then removed under vacuum to give a yellow oil.

Yield = 9.18g (90%).

^{1}H NMR (360 MHz $CDCl_3$): δ = 0.092 ppm (s, 6H, $SiCH_3$), 0.933 ppm (s 9H t-but), 3.8 ppm (s, 3H, OCH_3), 4.78 ppm (s, 2H, Ar-CH_2), 7.36 ppm (d, 2H, aromatic protons), 7.98 ppm (d, 2H, aromatic protons).

4. 4-(Tert-butyl-dimethyl-silanyloxymethyl)-phenyl (8)

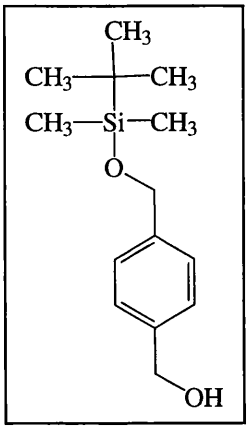

Compound **8** was prepared using the method of De Shong and co-workers[6]. To a solution of **7** (9.18g, 0.0327mol) in dry diethyl ether (56ml) under N_2, lithium aluminium hydride (0.625g, 0.01647mol) was added portionwise with stirring. The solution was then brought to reflux and left for 1 hour after which the solution was allowed to cool and the reaction quenched with water and neutralised with 6M hydrochloric acid. The product was then extracted into ether and the organic layers dried over magnesium sulphate. The solvent was then removed to give a yellow oil.

Yield = 5.51g (66.7%).

^{1}H NMR (360 MHz $CDCl_3$): δ = 0.08 ppm (s, 6H, $SiCH_3$), 0.92 ppm (s, 9H, t-bu), 4.65 ppm (s, 2H, $ArCH_2OH$), 4.72 ppm (s, 2H, $ArCH_2Si$), 7.31 ppm (s, 4H, aromatic protons).

5. 2-(4-Bromomethyl-benzyloxy)-tert-butyl-dimethyl-silanyloxymethyl (9)

Attempt A

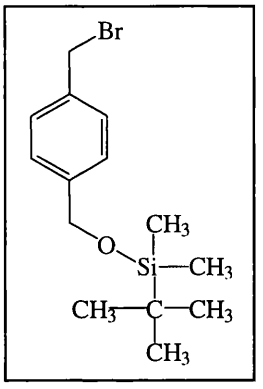

To a solution of **8** (1.08g, 4.29mmol) in dichloromethane (20ml) was added drop wise tri-methylsilylbromide (1.14ml, 6.42mmol). After 10 minutes of stirring a white solid was formed and filtered, from NMR analysis it was found that both the hydroxide group and the protected hydroxide group had been brominated.

Attempt B

To a solution of **8** (1g, 4.29mmol) in dry toluene (150ml) and dry diethyl ether (50ml) was added drop wise phosphorous tribromide (1.6ml, 17mmol) in dry toluene (25ml), and left stirring overnight. The solvent was then removed and the residue dissolved in chloroform and washed with water. The organic layer was then collected, dried over magnesium sulphate and the solvent removed to give a white solid. After NMR analysis it was found that both the hydroxide group and the protected hydroxide group had been brominated.

6. Methyl 4-[(tetrahydropyran-2-yloxy)methyl]benzoate (4)

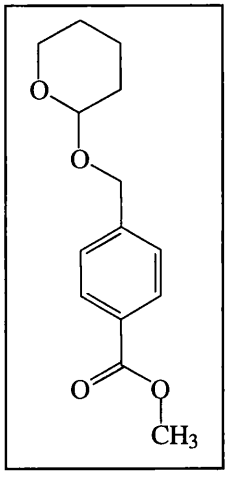

Compound **7** was prepared using the method outlined in Vogel.[7] To a solution of **3** (5g, 0.3mol) in dry dichloromethane (210ml) was added 1,3-dihydropyran (2.53g, 0.03mol) and PPTS (0.752g, 0.003mol). The mixture was left stirring overnight at room temperature after which the solution was diluted with water and washed with half-saturated brine to remove the PPTS. The organic layer was then dried over magnesium sulphate and the solvent removed under vacuum to give the product.

Yield = 7.52g (99%).

^{1}H NMR (360 MHz $CDCl_3$): δ = 1.55 ppm (multiplet, 8H, protons on the pyran), 3.89 ppm (s, 3H, OCH_3), 4.52 ppm (d, 1H, CH of CH_2), 4.74 ppm (s, 1H, CH on pyran), 4.82 ppm (d, 1H, CH of CH_2), 7.41 ppm (d, 2H, aromatic protons), 7.9 ppm (d, 2H, aromatic protons).

7. 4-(Tetrahydro-pyran-2-yloxymethyl)-phenyl (5)

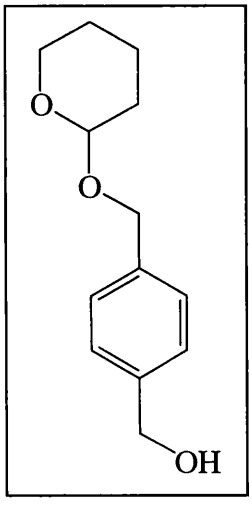

To a solution of **4** (7.25g, 0.031mol) in dry tetrahydrofuran under N_2 was added lithium aluminium hydride (2.9g, 0.76mol) portion wise with stirring. The mixture was then brought to reflux and left for 3 hours after which the solution was allowed to cool to room temperature and filtered. The product was then extracted into chloroform and the organic layers dried over magnesium sulphate. The solvent was then removed under vacuum to give a golden oil.

Yield = 4.4g, (63.9%).

^{1}H NMR (360 MHz $CDCl_3$): δ = 1.6 ppm (multiplet, 8H, protons on the pyran), 4.5 ppm (d, 1H, CH of CH_2), 4.69ppm (s, 2H, CH_2OH), 4.70 ppm (s, 1H, CH on pyran), 4.75 ppm (d, 1H, CH of CH_2), 7.24 ppm (s, 4H, aromatic protons).

8. 2-(4-Bromomethyl-benzyloxy)-tetrahydro-pyran (10)

Attempt A

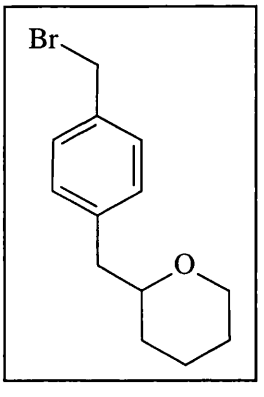

To a solution of n-bromosuccinamide (1.68g, 9mmol) in dry THF (100ml) was added triphenylphosphine (2.5g, 9mmol) in dry THF drop wise over 30 minutes. This caused a precipitate to form to which **5** (2g, 9mmol) in dry THF was added drop wise and left for 1 hour 15 minutes after which the precipitate that had formed had gone into solution. The solvent was then removed and the residue taken up into a mixture diethyl ether and water. The organic layer was then collected, washed with water and dried over magnesium sulphate. The solvent was then removed to give an orange solid. The impure product was then purified via column chromatography; silica gel eluant dichloromethane/methanol 98:2. This did not result in good separation although T.L.C. had indicted good separation.

Attempt B

To a solution of **5** (2.4g, 10.8mmol) in dry toluene (150ml) and dry diethyl ether (50ml) was added drop wise phosphorous tribromide (1ml, 10.8mmol) in dry toluene (25ml), and left stirring overnight. The solvent was then removed and the residue dissolved in chloroform and washed with water. The organic layer was then collected, dried over

magnesium sulphate and the solvent removed to give a white solid. NMR analysis revealed that both the hydroxide group and the protected hydroxide group had been brominated.

9. 4-(Bromomethyl) benzyl alcohol (6)

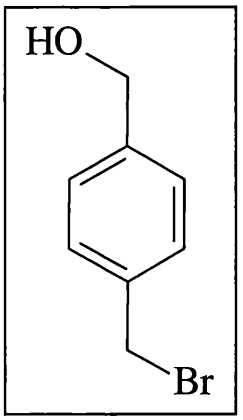

Compound **6** was prepared by the method of Bayle-Lacoste and co-workers[4]. To a solution of lithium aluminium hydride (5.7g, 0.15 mol) in diethyl ether (300 ml) at a temperature between -10° and -15° was added slowly with stirring aluminium chloride (6.68g, 50mmol). This mixture creates an *in situ* solution of aluminium hydride to which **2** (23.18g, 0.1mol) was slowly added and allowed to come to room temperature and stirred for 2 hours. After this time the solution was cooled to -10° and the product liberated via addition of saturated sodium sulphate solution. The solution was then filtered, dried over magnesium sulphate and the solvent evaporated to dryness under vacuum without heating. The resulting white solid that was left had to be used rapidly for the following step, as the product is unstable.

Yield = 15g (75%).

10. 2-(4-Bromomethyl-benzyloxy)-tetrahydro-pyran (10)

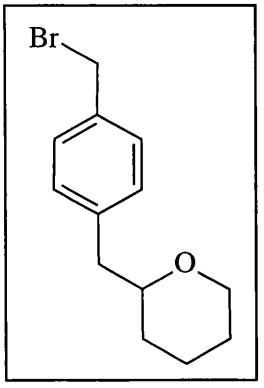

A solution of **6** (15g, 74.8 mmol), dihydropyran (6.28g, 74.8 mmol) and PPTS (1.87g, 7.48 mmol) in DCM (210 ml) was left stirring overnight. After which the solution was diluted with ether and washed with half-saturated brine. The ethereal layer was then dried over $MgSO_4$ and concentrated in vacuo.

Yield = 20.36g (95.5%).

^{1}H NMR (360 MHz, $CDCl_3$): δ = 1.55 ppm (multiplet, 8H, Pyran H), 4.43 ppm (s, 2H, CH_2-Br), 4.5 ppm (s, 2H, CH_2-pyran), 4.7 ppm (d, 1H, CH on pyran), 7.29ppm (d, 2H, aromatic H), 7.48 ppm (d, 2H, aromatic H).

E.I. mass spectrometry: m/z = 277 (M^+).

11. 2-Methyl-3-(methyl-4-benzyl alcohol)-benzoxazolium-bromide (BS1)

Method A

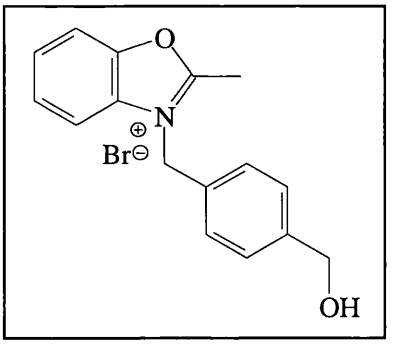

10 (9g, 32 mmol) and 2-methyl-benzoxazole (4.2g, 32 mmol) were placed in a round-bottomed flask and stirred together at 120°C until a brown solid formed after approximately 1 to 2 hours. The reaction was then allowed to cool to room temperature whereupon several purification methods were attempted and are outlined below.

1. Recrystilization.

   The product was found to be very insoluble in many solvents except for methanol and ethanol. The product was dissolved in ethanol and attempts to precipitate it with a solvent of lower polarity only resulted in brown impure salts.

2. Conversion of the counter ion to PF_6.

It was thought that by converting the bromide counter ion to hexaflourophosphate would be a viable way of purifying the salt. This was attempted by dissolving the salt in water and adding ammonium hexaflouro phosphate to precipitate it as the pure product. This strategy also failed as it was found that the product was sparingly soluble in water.

3. Chromatography.

A silica column was tried but did not give adequate separation. Ion exchange columns were considered but dismissed as the product is sparingly soluble in water.

^{1}H NMR (360 MHz, d_6-DMSO): δ = 1.76 ppm (s, 3H, CH_3), 4.09 ppm (d, 1H, CH_2), 4.11 ppm (d, 1H, CH_2-OH), 5.21 ppm (d, 1H, CH_2), 5.23 ppm (d, 1H, CH_2-OH), 6.71 ppm (t, 1H, aromatic H), 6.9 ppm (t, 2H, aromatic H), 7.09 ppm (t, 1H, aromatic H), 7.35 ppm (d, 2H, aromatic H).

E.I. mass spectrometry: m/z = 254 (M-Br)

Method B

As the attempts to purify the product in method A failed an alternative method was attempted. **10** (1g, 3.51 mmol) and 2-methyl-benzoxazole (0.467g, 3.51 mmol) were placed in a round bottom flask and dissolved in toluene (50 ml). The reaction was stirred at reflux for 12 h after which point no precipitate had formed as predicted. The solvent was then removed in vacuo leaving yellow oil which was identified by NMR spectroscopy as being the starting materials, i.e. no reaction had occurred.

This method was then repeated twice using chlorobenzene and acetonitrile as solvents but as before no reaction took place.

2.3.2.2 Reaction Scheme 2

1. α-Bromo-*p*-tolualdehyde (12)

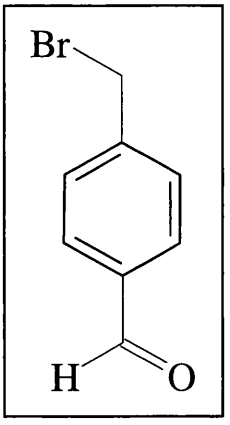

Compound **12** was prepared by the method of Wen and co-workers[8], with one difference the DIBAL-H was in toluene and not hexane. 4-(Bromomethyl)-benzonitrile (4.34g, 22mmol) was dissolved in toluene and cooled to 0°C under N_2. Then DIBAL (21ml) was added drop wise and the solution allowed to stir for 1 hour, after which chloroform (80ml) and 10% hydrochloric acid (200ml) were added and the solution allowed to stir for a further hour. After this time the organic layer was extracted and washed with water. The solution was then dried over magnesium sulphate, filtered and the solvent almost fully removed under vacuum. The remaining solvent was then placed in a fridge where upon the product precipitated to give a white solid that was filtered and washed with hexane.

Yield = 2.41g (55%)

^{1}H NMR (360 MHz, $CDCl_3$): δ = 4.50 ppm (s, 2H, CH_2-Br), 7.53-7.55 ppm (d, 2H, atomatic protons), 7.84-7.86 ppm (d, 2H, atomatic protons), 10.00 ppm (s, 1H, CH=O).

2. α-1,4,7-triazatricyclo[5.2.1.0]decane-*p*-tolualdehyde (20)

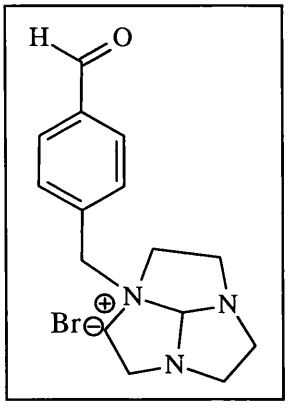

To a solution of α-Bromo-*p*-tolualdehyde **20** (1g, 5mmol) in methanol (25ml), under N_2 and at r.t., was added drop wise 1,4,7-triazatricyclo[5.2.1.0]decane (0.695g, 5mmol) in methanol (25ml). The reaction was left stirring overnight where upon a white solid precipitated. The precipitate was then filtered and dried under

vacuum.

Yield = 0.91g (53.85%).

^{1}H NMR (360 MHz, d6-DMSO): δ = 2.8-3.2 ppm (multiplet, 12H, capped-TACN-H), 4.5 ppm (s, 1H, capped-TACN-H), 5.4 ppm (s, 2H, CH_2-TACN),7.6 ppm(d, 2H, aromatic H), 7.89 ppm (d, 2H, aromatic H), 10.01 ppm (s, 1H, CH=O).

3. N-(p-Bromomethylbenzylidene)-2-aminophenol (13)

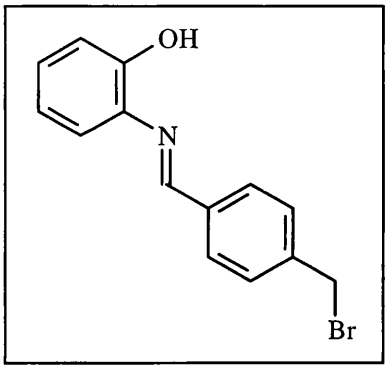

To a solution of α-Bromo-*p*-tolualdehyde **13** (1g, 5mmol) in methanol (25ml), at r.t., was added drop wise 2-aminophenol (0.55g, 5mmol) in methanol (25ml). The reaction was left stirring overnight where upon a dark brown solution was formed and then used immediately for the next step.

4. N-(p-Bromomethylbenzyl)-2-aminophenol (14)

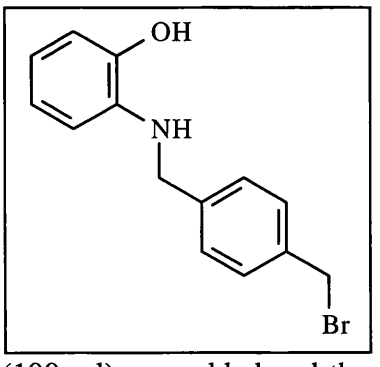

The solution obtained from the previous step was warmed to about 40°C and with stirring $NaBH_4$ (0.2g, 5mmol) was added portion wise, over a period of 30 min. A steady evolution of hydrogen occurred and the reaction was then heated to reflux for a further 15 min. After which time water (100 ml) was added and the solution allowed to cool to r.t.. After the reaction had cooled the solvent was removed and the crude product purified by column chromatography (SiO_2,

dichloromethane). Chromatography gave two bands that when analysed by NMR spectroscopy showed the product had in some way degraded on the column.

2.3.2.3 Reaction Scheme 3

1. 2-Methyl-3-(4-methyl benzoate)-benzoxazolium-bromide (BS6)

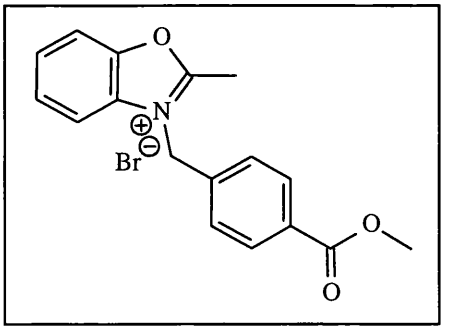

Bromomethyl 4-methyl benzoate (**2**) (1.3g, 5.677 mmol) and 2-methyl-benzoxazole (0.78g, 5.865 mmol,) were placed in a round-bottomed flask and stirred together at 120°C until an orange solid formed after approximately 1 hour. The reaction was then allowed to cool to room temperature and the orange solid triturated with diethyl ether, to yield a white solid that was collected via filtration and dried under vacuum.

Yield = 1.277g (63.85%).

^{1}H NMR (360 MHz, $CDCl_3$): δ = 1.78 ppm (s, 3H, CH_3), 3.8 ppm (S, 3H, O-CH_3), 4.33 ppm (d, 1H, CH of CH_2), 5.21 ppm (d, 1H, CH of CH_2), 6.7 ppm (t, 1H, aromatic H), 6.91 ppm (t, 2H, aromatic H), 7.1 ppm (t, 1H, aromatic H), 7.3 ppm (d, 2H, aromatic H), 7.8 ppm(d, 2H, aromatic H).

E.I. mass spectrometry: m/z = 333 (M-(O-CH_3))

2. 3-{2-[4-(1,3-dibutyl-4,6-dioxo-2-thioxo-tetrahydro-pyrimidin-5-ylidene)-but-2-enylidene]-benzooxazol-3-yl}-4-methyl benzoate (MC3)

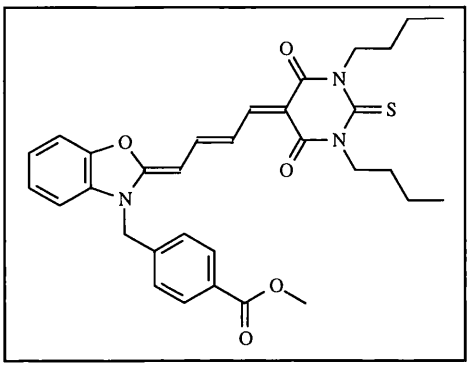

To a solution of compound **BS6** (277mg, 0.7647mmol) and 1,3-dibutyl-5-(3-ethoxy-allylidene)-2-thioxo-dihydro-pyrimidine-4,6-dione (260mg, 0.7647mmol,) in methanol (100 ml), was added triethylamine (a few drops). The reaction mixture was then stirred at reflux overnight, after which time a deep purple solution formed indicating the formation of the product. The solvent was then removed in vacuo leaving the crude product which was dried under vacuum.

The crude product was purified by column chromatography [SiO_2, ethyl acetate/ hexane 1:1] then due to incomplete separation a second column was needed [SiO_2, diethyl ether.].

Yield = 0.16g (36.51%).

^{1}H NMR (400 MHz, $CDCl_3$): δ = 0.88 ppm (t, 6H, CH_3), 1.3 ppm (tq, 4H, CH_2), 1.6 ppm (tt, 4H, CH_2), 3.85 ppm (s, 3H, OCH_3), 4.36 ppm (t, 4H, N-CH_2-CH_2), 5.08 ppm (s, 2H, CH_2), 5.45 ppm (d, 1H, =CH-), 7.01 ppm (multiplet, 2H, aromatic H), 7.21 ppm (t, 2H, aromatic H), 7.23 ppm (t, 2H, aromatic H), 7.39 ppm (multiplet, 1H, aromatic H), 7.7 ppm (dd, 1H, =CH-), 7.82 ppm (dd, 1H, -CH=), 7.9 ppm (s, 1H, -CH=), 7.98 ppm (t, 2H, aromatic H).

E.I. mass spectrometry: m/z = 573.3 (M^+)

3. 3-{2-[4-(1,3-dibutyl-4,6-dioxo-2-thioxo-tetrahydro-pyrimidin-5-ylidene)-but-2-enylidene]-benzooxazol-3-yl}-4methyl benzoic acid (MC4)

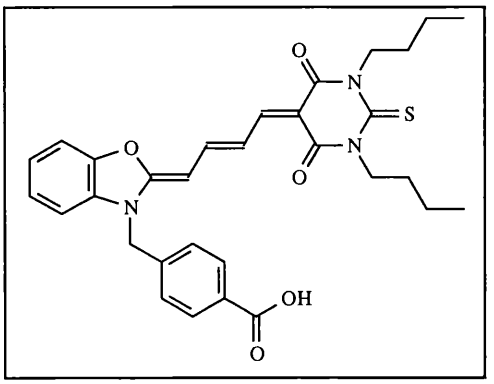

To a solution of **MC3** (13.5mg, 0.023 mmol) in methanol, at r.t. , was added drop wise NaOH (1.88mg, 0.047 mmol) in methanol. The reaction was stirred at room r.t. and after 30 min the solution turned from purple to orange indicating the breakdown of the polymethine backbone.

References

1: Benniston A. C., Harriman A., Romero F. M., Ziessel R., *J. Phys. Chem.*, **1999**, 103, 5399.

2: Benniston A. C., Harriman A., Mackie P. R., *Tetrahedron Lett.*, **1997**, 38, 3577.

3: Mackie P. R., *Cation Chelating [2]Catenanes and Cyclophanes based on 2,2` Bipyridine*, PhD *Thesis*, University of Glasgow, UK, 1998, pp84.

4: Bayle-Lacoste M., Boumekouez A., Collignon N., Moulines J., Neuzil E., Tinguț-Moreaud E., *Tetrahedron*, **1990**, 46 (23), 7793.

5: Vogel A. I.,*Vogels` Textbook of Pratical Organic Chemistry*, 5th ed, rev. by Furniss B. S., Hannaford A. J., Smith P. W. G., Tatcher A.R., Longman Group UK limited, 1989 pp461.

6: DeShong P., Hill D. K., Pilcher A. S., Shimshock S. J., Waltermire R. E., *J. Org. Chem.*, **1992**, 57, 2492.

7: Vogel A. I.,*Vogels` Textbook of Pratical Organic Chemistry*, 5th ed, rev. by Furniss B. S., Hannaford A. J., Smith P. W. G., Tatcher A.R., Longman Group UK limited, 1989 pp552.

8: Li M., Schlenoff J. B., Wen L., *J. Am. Chem. Soc.*, **1997**, 119 (33), 7726.

CHAPTER 3

Functionalized Ruthenium(II) Polypyridyl Complex

3.1 Introduction

Polypyridyl complexes of second and third row transition metal ions such as ruthenium(II), osmium(II), rhenium(I) and iridium (III) have been the focus of attention for many years, particularly considering their interesting and beneficial electrochemical and photophysical properties.[1-6] Without a doubt the complex $[Ru(bipy)_3]^{2+}$ (bipy = 2,2'-bipyridyl) has been the most extensively studied complex of this type due to its relatively long-lived excited state lifetime which readily emits at room temperature in a range of solvents. The photophysical properties of this complex are now generally well understood, with emission occurring from a triplet metal-to-ligand charge-transfer (^{3}MLCT) state which is formulated as $[Ru(III)(bipy)_2bipy^-)]^{2+}$ and in which the promoted electron resides in the LUMO of a single bipy ligand.[7] The quenching of the luminescence from $[Ru(bipy)_3]^{2+}$ has been extensively studied using a wide range of reagents, and occurs via either oxidative/reductive electron transfer or energy transfer processes.[8] By building secondary binding sites such as crown ethers,[9] cyclodextrins[10] azamacrocycles[11] and pH receptive groups[12-14] onto the core of the "Ru(biby)$_3$" the beneficial aspects of this quenching have been harnessed for applications within the field of chemical sensors. At present an abundance of luminescent probes such as this exist, however detailed studies into their basic photophysical properties often reveal interesting and unexpected results. For instance, Hupp *et. al.* [15] observed that the excited state lifetime of the complex (**C1**) increased, despite the presence of the pyridinium group attached directly to the

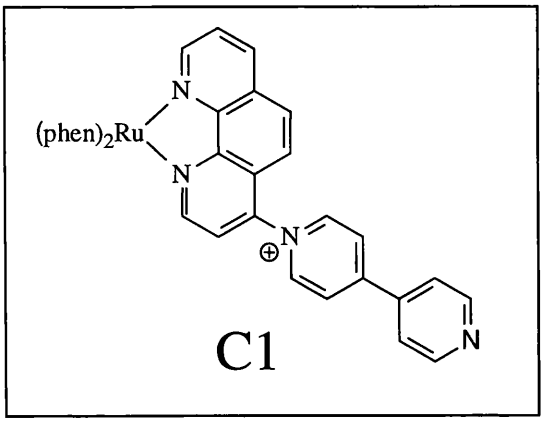

C1

phenanthroline ligand. Another observation noted by the addition of the pyridinium group, was that of a small red shift in the corrected luminescence energy maximum.

This chapter gives a detailed temperature and solvent dependence investigation of a ruthenium(II) polypyridyl complex (**C2**) similar to that reported by Hupp. In the case of complex (**C2**), however, the 4-pyridinium-4'-pyridine group is connected via a methylene spacer to a bipy group that is bound to the metal and observed solvent effects are considered to occur by way of through-space interactions.

3.2 Discussion of synthesis

The synthesis of $\mathbf{L_1}$ is depicted in Scheme 3.1 and is the precursor in the manufacture of more elaborate catenane and cyclophane derivatives.[16] The synthesis of the ruthenium complex was carried out prior to my involvement in the project, however the initial concern was that of the of an enatiomerically pure ruthenium complex. In order to achieve this $\mathbf{L_1}$ was refluxed in an ethylene glycol/water mixture with one equivalent of Λ-cis-[Ru(bipy)$_2$(pyridine)$_2$][(+)-*O,O'*-dibenzoyl-L-tartrate].[17] As well as forming the desired complex (**C2**) a number of other side products were obtained as shown by thin layer chromatography. These other products are believed to be larger aggregates formed by the complexation of the ruthenium(II) to the "free" nitrogen of the pyridyl groups. The desired compound (**C2**) was separated from all other side products by careful column chromatography (silica gel, MeOH/2N NH_4Cl/ $MeNO_2$ (7:2:1)) in a respectable 62% yield. The by-products have not yet been fully characterized. As no circular dichroism spectrum for (**C2**) could be obtained, it is believed that the complex racemized during silica gel chromatographic purification.

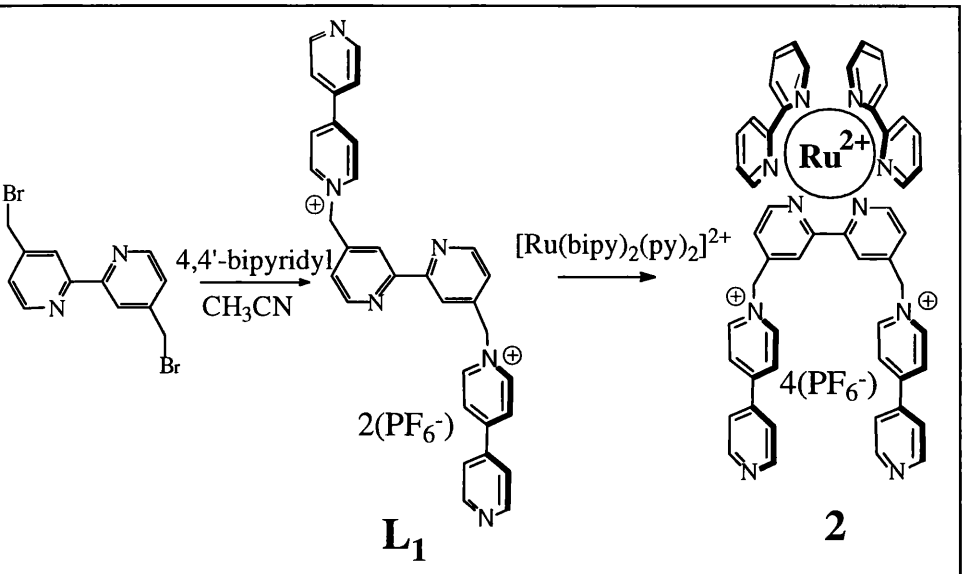

Scheme 3.1. Procedures used in the preparation of complex (**C2**).

3.3 Discussion of structure

The X-ray crystal structures of the ligand $\mathbf{L_1}$ and the complex **C2** have both been reported in P. R. Mackie's PhD thesis.[18a,b] However, the data for these structures has been reanalysed and are discussed in the following section.

Uncomplexed ligands based on bipy when in their low-energy conformation are described as *transoid* this is where the two nitrogens are *anti* to each other. The formation of this geometry is attributed to unfavourable electrostatic repulsion between the lone pair on the nitrogens, which forces the pyridine rings as far apart as possible. The molecular structure of the precursor ligand $\mathbf{L_1}$ clearly demonstrates this point. It can be seen that the *transoid* configuration places the two *N*-methylene-4-pyridinium-4'-pyridine cation units approximately 180° apart. As observed in other structures[19] the two *N*-methylene-4-pyridinium-4'-pyridine cations are non-planar with a torsion angle of *ca* 32°.

When complexed to the "Ru(bipy)$_2$" unit the ligand $\mathbf{L_1}$, is as expected forced into the *cisoid* conformation. The molecular structure of which shows that in this case the torsion angle between the nitrogen atoms of the 2,2'-bipyridyl group is now only *ca.* 2°.

The coordination geometry around the ruthenium ion can be seen as a distorted octahedron, this can be determined by studying the selected bond lengths and angles that are collected in Table 3.1. The average Ru-N bond distance is 2.06 Å, and typical for bipy-based complexes of dicationic ruthenium.[20] As viewed in the precursor ligand $\mathbf{L_1}$ the *N*-methylene-4-pyridinium-4'-pyridine cation moieties are non-planar with torsion angles of 11.8° and 26.7° which indicates a lack of double-bond character in the central C-C bond joining the two pyridine groups. This therefore supports that there is no electron migration from the "free" nitrogen to the electron deficient cationic nitrogen, at least not in the ground state. Furthermore, in the ground state the two "free" nitrogen ends of the *N*-methylene-4-pyridinium-4'-pyridine unit do not interact with one another as they are well separated (~ 6.5 Å). Therefore it is possible to treat each bipyridinium arm of the complex as an independent unit, when the photophysical properties of complex (**C2**) are discussed.

The methylene units connecting the bipy and 4-pyridinium-4'-pyridine groups have angles of 108.6° and 108.9° showing that they are almost tetrahedral in geometry. As a result of this the closest contact distance between the quaternary pyridinium nitrogen and bipy ligand is only *ca.* 2.4Å. This resulting closeness of the arrangement of these groups allows for a through-space interaction between them, especially when the complex is in the excited-state as an electron will be located in the LUMO of the bipy group.

	bond length(Å)		bond angle (o)
Ru(1)-N(100)	2.047(3)	N(100)-Ru(1)-N(210)	172.32(12)
Ru(1)-N(210)	2.053(3)	N(110)-Ru(1)-N(300)	173.31(13)
Ru(1)-N(110)	2.049(3)	N(310)-Ru(1)-N(200)	173.69(12)
Ru(1)-N(300)	2.056(3)	N(100)-Ru(1)-N(200)	95.03(12)
Ru(1)-N(200)	2.060(3)	N(100)-Ru(1)-N(110)	79.26(12)
Ru(1)-N(310)	2.064(3)	N(100)-Ru(1)-N(300)	97.12(12)

Table 3.1 Selected bond distances and angles observed for complex **(C2)**.

3.4 Photophysical properties

The absorption and fully-corrected fluorescence profiles of complex (**C2**) and $[Ru(bipy)_3]^{2+}$ in acetonitrile for comparison can be seen in Figure 3.1. Complex (**C2**) exhibits the characteristic MLCT absorption band centred at 22,124 cm^{-1} and a corresponding fluorescence band centred at 14,822 cm^{-1} with a calculated Stokes' shift of 7302 cm^{-1}. It can be seen from the spectra that the MLCT absorption band for (**C2**) is both red-shifted and considerably broader than that for $[Ru(bipy)_3]^{2+}$. The broadening of the absorption band is attributed to the presence of another underlying MLCT state which must be associated with the functionalized bipy unit. The introduction of the electron withdrawing *N*-methylene-4-pyridinium-4'-pyridine cation onto the bipy backbone has resulted in the overall shift of the absorption band of **(C2)** to a lower energy, similar to that sceen by Hupp *et. al.* for **(C1)**. In view of this, the MLCT state is formulated as $[Ru(III)(bipy)_2(\mathbf{L_1}^-)]^{2+}$ but with the electron residing on the bipy portion of the functionalized ligand.

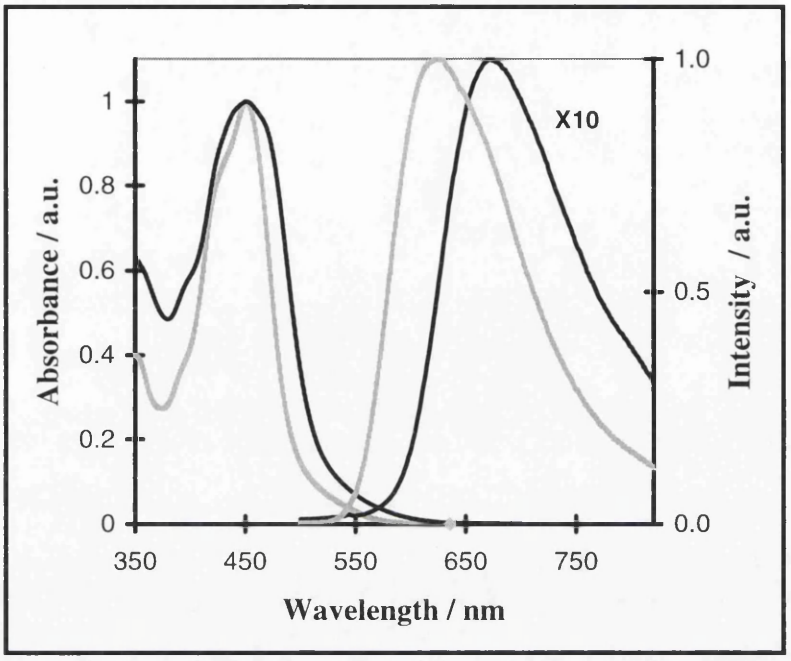

Figure 3.1 Absorption and fully-corrected fluorescence spectra of complex (**C2**) (dark line) and $[Ru(bipy)_3]^{2+}$ (dashed line) in acetonitrile at 22 °C.

Further delocalization of the electron onto the *N*-methylene-4-pyridinium-4'-pyridine unit to generate an extended superligand has been discounted since the connecting methylene will act as an insulator due to its lack of double bound characteristics. Furthermore, electron transfer to the *N*-methylene-4-pyridinium-4'-pyridine cation is also unlikely since this process is thermodynamically unfavourable by *ca.* 0.3 eV.

The fluorescence profile of **(C2)** was satisfactorily simulated using the expression 1 and can be seen in Figure 3.2.

$$I(E) = \sum_{\upsilon=0}^{N} \left(\frac{E_o - \upsilon\hbar\omega_m}{E_o} \right)^3 \left(\frac{(S_m)^\upsilon}{\upsilon!} \right) x \exp\left[-4\ln(2) \left(\frac{E - E_o + \upsilon\hbar\omega_m}{\upsilon_{1/2}} \right)^2 \right] \qquad \textbf{Eq. 1}$$

where I = intensity at wavenumber E, E_o = energy difference between 0,0 vibronic levels, $\hbar\omega_m$ = medium frequency vibrational mode, S_m = Huang-Rhys electron-vibrational

coupling constant and $\nu_{1/2}$ = half-height band width. In this and other calculations a good fit was obtained using n = 10.

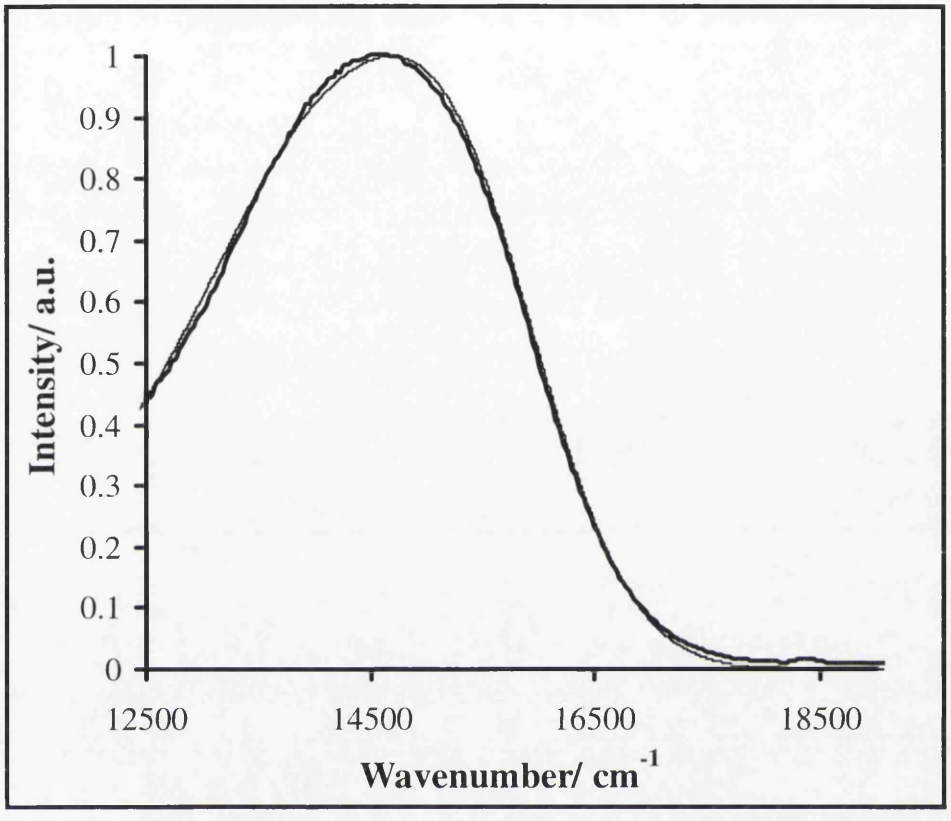

Figure 3.2 Normalized emission spectrum of complex (**C2**) in acetonitrile at 22 °C (solid line) and spectrum simulated using expression 1 shown in text (dashed line).

3.5 Solvent Effects

It is well established that solvent can play a key role in influencing the absorption and emission spectra of ruthenium polypyridyl complexes.[22] In the early work of Meyer and co-workers[23] solvatochroism displayed by complexes such as $[Ru(NH_3)_5(dmapy)]^{2+}$, where dmapy is 4-(dimethylamino)-pyridine, was attributed to solvent hydrogen-bonding to the ammine ligands. The net effect observed by the donation of an electron by the solvent

resulted in the increase of electron density on the metal, via the transfer of the electron through the ammine ligand to the metal centre. In this example the MLCT absorption band maximum correlated well with the Gutmann solvent donor number (DN) which represents the nucleophilic or donor properties of the solvent.[24] On the other hand solvent acceptor number (AN)[24] represents how well the solvent acts as an electrophile and its ability to act as an acceptor. Correlation of the absorption/emission spectra of $[Ru(phen)_2(CN)_2)]^{2+}$ and $[Ru(bpy)_2(CN)_2)]^{2+}$ explains their solvatochroism properties because of interaction of the solvent with the cyanide group.[25,26] In all the cases above the ligand which leads to the observed solvatochromic effects is directly attached to the metal ion centre and thus would be expected to affect the electronic properties of the complex. However since the appended *N*-methylene-4-pyridinium-4'-pyridine cation and bipy units are decoupled due to the presence of the methylene spacer unit, the solvent influence on electronic properties of complex (**C2**) was expected, at first, to be similar to $[Ru(bipy)_3]^{2+}$.[27] Thus, absorption and fluorescence spectra were recorded for (**C2**) in a range of solvents with varying DN, AN and polarity, and are collected in Table 3.2. Also summarized are the parameters obtained from band-shape analysis and fitting of the emission spectra using expression 1.

Solvent	E_{op} $(cm^{-1})^a$	E_{em} $(cm^{-1})^b$	Stokes'shift $(cm^{-1})^c$	E_o $(cm^{-1})^d$	$\nu_{1/2}$ $(cm^{-1})^e$	$\hbar\omega_m$ $(cm^{-1})^f$	S_m
CH_3CN	22124	14822	7302	15232	1950	1383	1.11
CH_2Cl_2	22173	15380	6793	15793	1950	1357	0.84
$(CH_3)_2CO$	21905	14936	6969	15418	1950	1353	0.95
$(CH_3)_2SO$	21834	15058	6776	15775	2100	1543	1.20
DMF[g]	21786	14755	7031	15599	2040	1312	1.30
BuCN[h]	21978	15077	6901	15442	1950	1416	0.78
CH_3NO_2	22026	14657	7369	14911	1990	1446	0.69
THF[j]	21930	14713	7217	15089	2050	1212	0.80
Pyridine	21787	15574	6213	16135	1820	1449	1.11
Formamide	21978	15032	6946	15683	2005	1331	1.05
MeOH	21978	15213	6765	15669	2150	1393	0.88
EtOH	21978	15337	6641	15847	2110	1355	0.91

Table 3.2 Solvent dependent parameters recorded for complex (**C2**) at 20°C in aerated samples.

Parameters as described in text. (a) ± 50 cm^{-1} (b) ± 50 cm^{-1} (c) ± 70 cm^{-1} (d) ± 20 cm^{-1} (e) ± 20 cm^{-1} (f) ± 20 cm^{-1} (g) N,N'-Dimethylformamide (h) Butyronitrile (j) Tetrahydrofuran

3.5.1 Solvent Polarity Effects

The effect a solvent has on an absorption spectrum is controled by the equilibrium ground state and the Frank-Condon excited state, whilst the fluorescence spectrum depends upon the equilibrium excited state and the Frank-Condon ground state. To this end the solvent polarity factor (Δf) introduced by Mataga[28,29] and Lippert[30] and used by other workers[31,32] allows a way to quantify the Stokes Shift (SS, in cm^{-1}) (Equations 2 and 3)

with the change in dipole moment between ground state (μ_g) and excited state (μ_e), induced by alterations in dipole-dipole interactions of the solvent and solute.

$$SS = \frac{2}{hc} \Delta f \frac{(\mu_e - \mu_g)^2}{a^3} \quad \textbf{Eq 2}$$

$$\Delta f = \left(\frac{D-1}{2D+1}\right) - \left(\frac{n^2-1}{2n^2+1}\right) \quad \textbf{Eq 3}$$

Here a = effective spherical radius (Å), D = static dielectric constant and n = refractive index.[33]

As illustrated in Figure 3.3 there is a good correlation between SS and Δf for the aprotic solvents of D >10, with an increasing in the SS as the solvent polarity increases.[34] The strong solvent dependence of (**C2**) in aprotic media supports a considerable dielectric reorganization of the solvents and is found to give similar results as those found for $[Ru(bipy)_2(CN)_2]$.

By using the slope shown in Figure 3.5 the change in dipole moment (μ_e-μ_g) was calculated as *ca.* 29D[37] for a = 8.8Å; with a radius of this size all ligand parts within the complex are incorporated. This high value suggests that it is a gross overestimate since the transition dipole is only incorporated within the the bipy section within the complex. For example, the corresponding (μ_e-μ_g) value of $[(NH_3)_5Ru(4,4'\text{-bipyH})]^{3+}$ is only *ca.* 17D.[22] When the 4-pyridinium-4'-pyridine group attached to the bipy section is ignored then a more reasonable estimate using a ~ 4.4Å results in a change of dipole moment of *ca.* 10 D, which is approximately half the theoretical calculated value. This lower than expected value is in good correlation with previous work on related systems and has been determined to occur as a result of electron delocalization and polarization of the ligand electrons.[22]

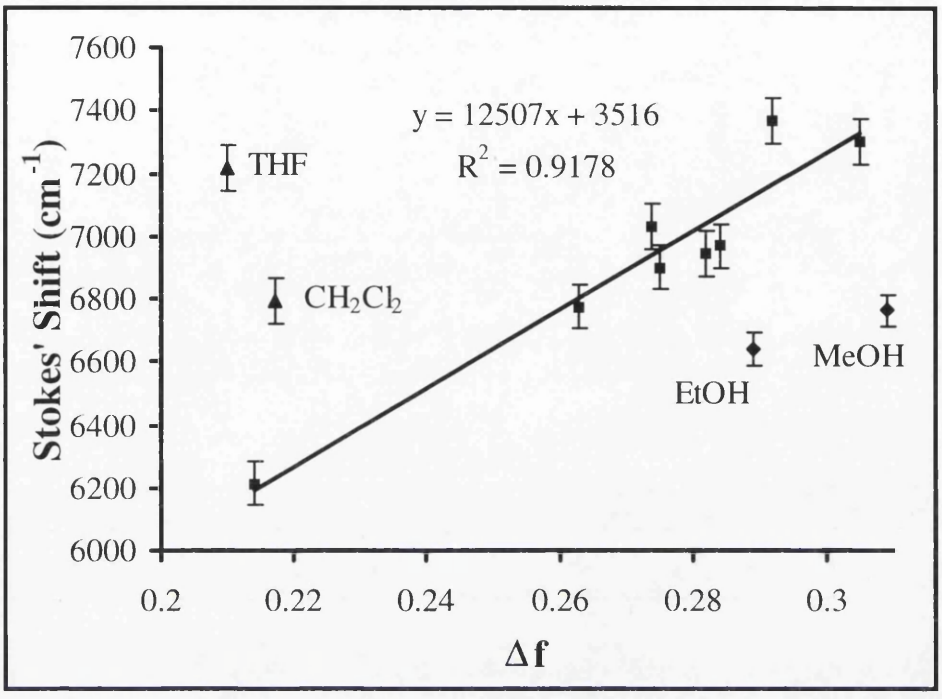

Figure 3.3 Plot of Stokes' shift versus solvent polarity function Δf for complex (**C2**) in a range of solvents at 22 °C. Insert shows least-squares straight line fit to data points and goodness-of-fit parameter.

3.5.2 Solvent Donor Number

The optical parameters found for (**C2**) were found to be unrelated to the Gutmann's solvent AN. As the only site for solvent interactions is the "free" nitrogen of the *N*-methylene-4-pyridinium-4'-pyridine group, it is fair to say that this site does not significantly control the photophysical properties of the complex. However there was a noticeable dependence between the absorption/emission data and the calculated parameters obtained using equation 1 with Gutmann's DN (Table 3.2). This relationship was found to be that with increasing DN, values of emission maximum (E_{em}) and E_o (Figure 3.4a) increased whilst in contrast the absorption maximum (E_{op}) values decreased (Figure 3.4b).

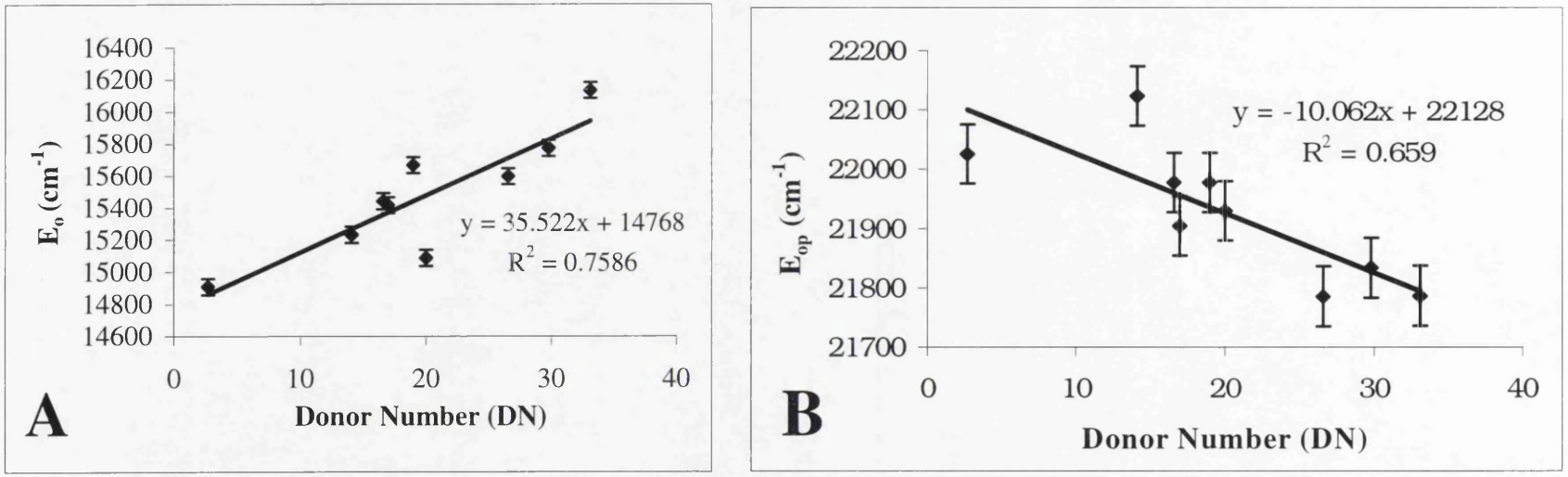

Figure 3.4a and 3.4b Plots of E_o and E_{op} respectively versus Gutmann's solvent donor number for complex (**C2**). Insert shows least-squares straight line fit to data points and goodness-of-fit parameter.

As can be seen in Figure 3.5 there was to be a satisfactory linear correlation between (E_{op}-E_o) and DN, and indicates that the energy difference between the first-excited ^{1}MLCT and ^{3}MLCT states decreases with increasing DN.

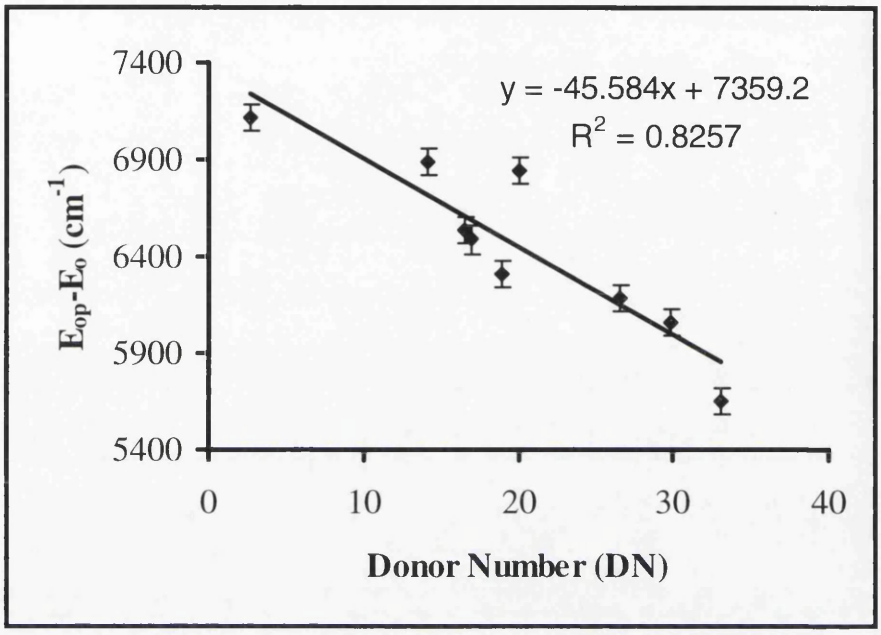

Figure 3.5 Plot of (E_{op}-E_o) versus Gutmann's solvent donor number for complex (**C2**). Insert shows least-squares straight line fit to data points and goodness-of-fit parameter.

Although less specific it was also found that the calculated Huang-Rhys (S_m)[36] values did also gradually increase with increasing DN (Figure 3.6). Since S_m is related to the equilibrium configurations of the ground and excited states by the dimensionless fractional displacement parameter (Δ_j) (Equations 4 and 5), this suggests that the structure of the acceptor ligand in the complex does change slightly depending on the donor ability of the solvent. Furthermore, since the extent of mixing between ground and excited state will decrease, (this decrease in mixing is a result of the increased energy gap between the

two states) the result will be a greater degree of charge transfer to the acceptor ligand in the excited state.[37,38]

$$S_m = \frac{1}{2}\sum_j \Delta_j^2 \quad \textbf{Eq. 4}$$

$$\Delta_j = \left(Q_o^g - Q_o^e\right)\left(m\varpi_j / \hbar\right)^{1/2} \quad \textbf{Eq. 5}$$

Where m = reduced mass, Q_o^e and Q_o^g represent the excited and ground state equilibrium positions, respectively.

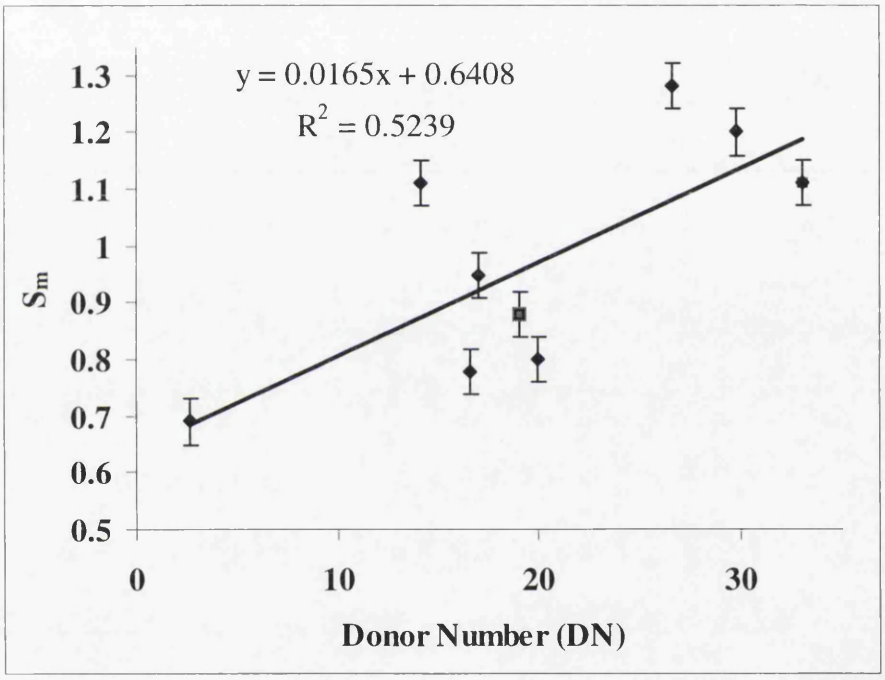

Figure 3.6 Relationship between Huang-Rhys factor (S_m) and solvent donor number (DN) for $[Ru(bipy)_2L_1]^{2+}$. Insert shows equation of least-squares straight line fit through the data points and goodness of fit parameter.

3.5.3 Nature of Solvent-Solute Interaction

As for this case the nature of the solvent effect is that of donation, it is clear that the solvent must interact with complex (**C2**) at a site where the complex is electron deficient and able to act as an acceptor. Taking this into consideration the most electron deficient site within the complex is the cationic nitrogen of the *N*-methylene-4-pyridinium-4'-pyridine group. It is at this location that the interaction is most likely to take place as illustrated in the simplified excited-state diagram below.

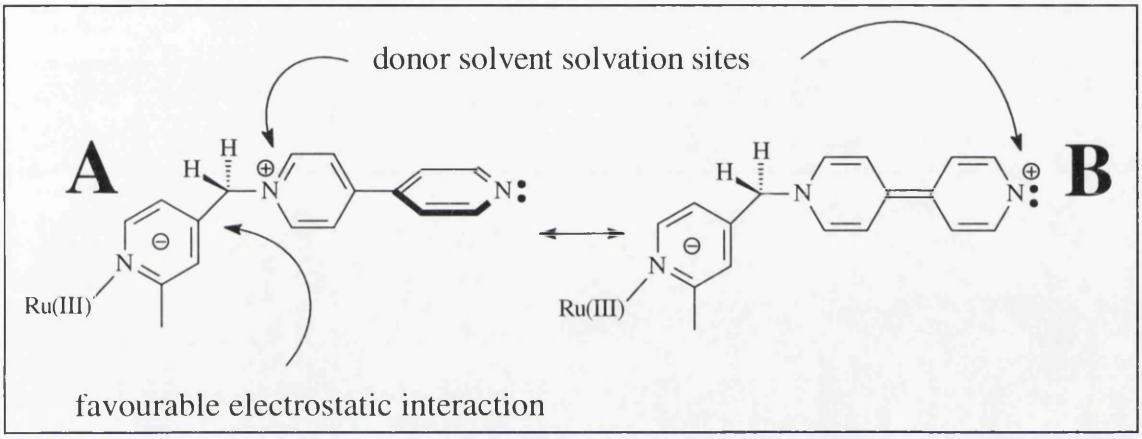

Since excitation of the complex will result in an electron being located in the bipy section of the functionalised ligand then the resonance form **A** would be the more favoured by a simple electrostatic argument. This is also supported by the examination the X-ray crystal structure, which shows a lack of double bond character in the C-C bound connecting the pyridine groups. The outcome of solvent donation to the resonance form **A** would be a reduction in the positive charge at the nitrogen, and would then result in the de-stabilisation of the excited state. It would therefore follow that the energy of the excited state would rise with increasing DN. Unfortunately, the effect of the solvent on the ground state is less clear.

3.5.4 Potential Energy Surface Model

A simplified potential-energy surface diagram can now be created in order to incorporate all the previous results, which occur due to the changes in solvent donation (Figure 3.7). The key features of the model that are worth noting are: In order to increase E_o with DN along with allowing a decrease in E_{op} there has to be an increase in energy of the ^{3}MLCT state coupled to a lowering in energy of the ^{1}MLCT state. As well as $\Delta Q' > \Delta Q$ for the ^{3}MLCT state and accounts for structural alteration in the acceptor ligand.

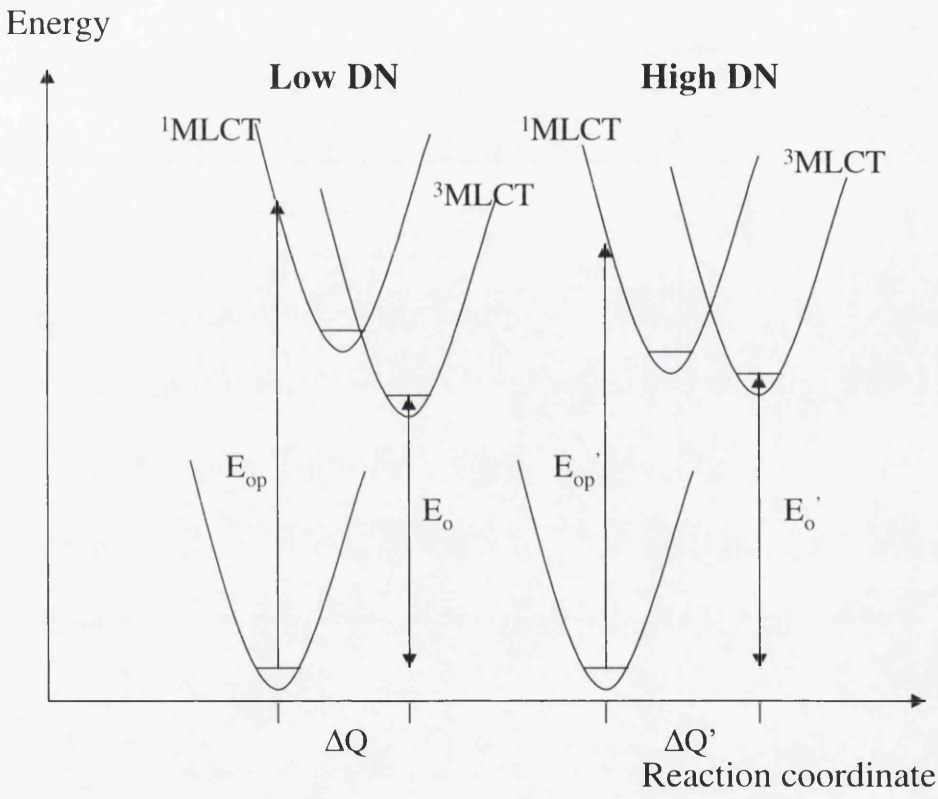

Figure 3.7 A simplified potential-energy surfaces diagram for (**C2**) in a solvent of low and high donor number.

3.6 Temperature Dependency Studies

The observed rate constant (k_{obs}) for decay of the excited state in $[Ru(bipy)_3]^{2+}$ over a modest temperature range can be fitted to a three term expression (Eq. 6), and is pictorially shown in Figure 3.8.

$$k_{obs} = k_{nr} + k_r + A' \exp\left(\frac{-\Delta E}{RT}\right) \qquad \textbf{Eq. 6}$$

Where k_{obs} = observed rate constant for excited state decay, k_{nr} = non-radiative decay constant, k_r = radiative decay constant, A' = pre-exponential factor associated with deactivation from the d-d state and ΔE = activation energy. Because of the thermally-activated deactivation process the Arrhenius plot for $[Ru(bipy)_3]^{2+}$ is typically curved over the range 233K to 303K affording a ΔE value in acetonitrile of 3800 cm^{-1}.

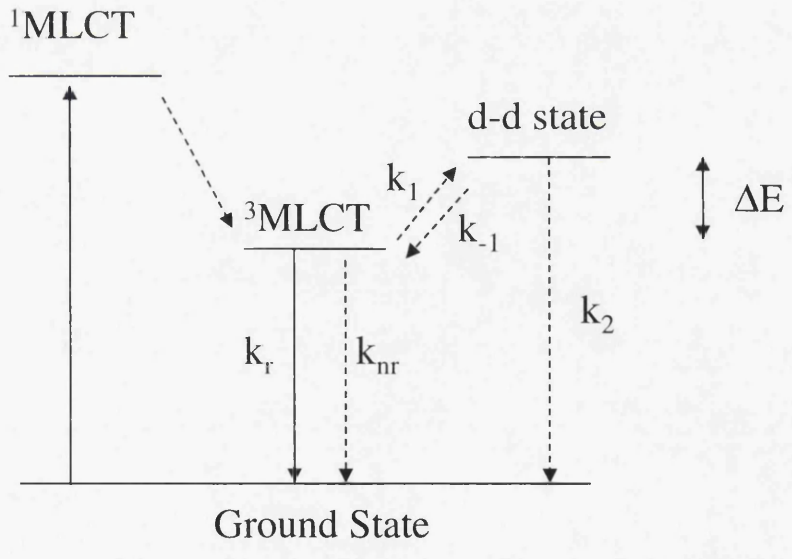

Figure 3.8 Excited-state deactivation model for ruthenium(II) polypyridyl complexes. Meaning of symbols is explained in the text.

Figure 3.9 illustrates the Arrhenius plot for (**C2**) in acetonitrile over the temperature range 274K to 333K. It can be seen from this plot that there is a definite lack of curvature, unlike that observed for the plot of $[Ru(bipy)_3]^{2+}$. This would suggest that the model shown in Figure 3.8 is not applicable for the complex (**C2**). Indeed, the ΔE value as calculated from the least-squares fit to the gradient is only 464±5 cm^{-1} with a corresponding pre-exponential factor (A) of 3.5 x 10^7 s^{-1}.

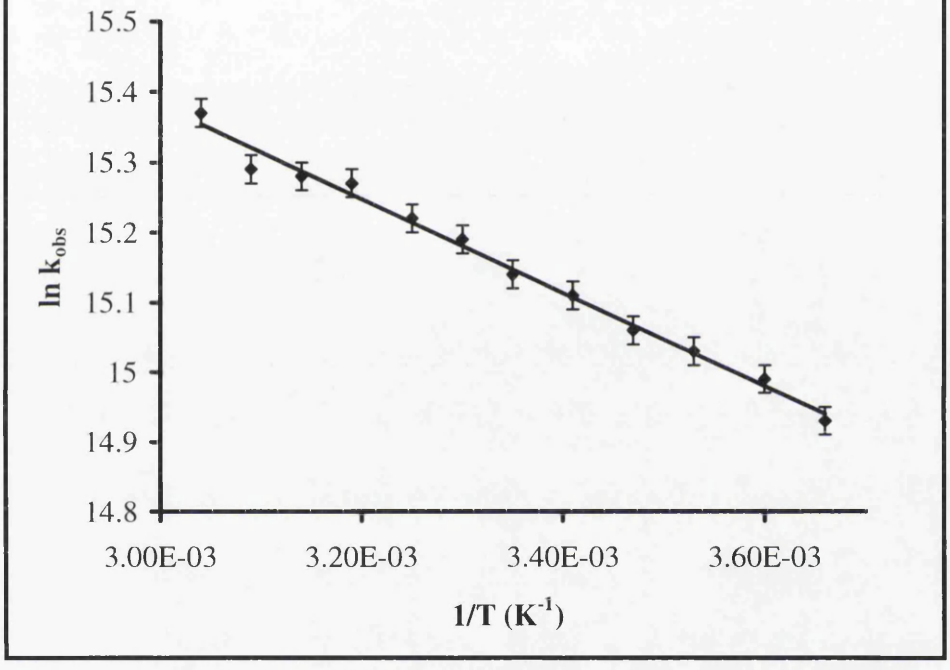

Figure 3.9 Arrhenius plot of $\ln k_{obs}$ versus 1/T for (**C2**) in acetonitrile.

As depicted in Figure 3.8 the deactivation of the MLCT state via the d-d excited state can be explained in terms of three competing processes such that:

$$k' = k_1\left(\frac{k_2}{k_{-1} + k_2}\right) \text{ where } k' = A'\exp\left(\frac{-\Delta E}{RT}\right)$$

It is clear to see that a number of cases exist depending on the relative values of the three rate constant terms. In the first case scenario $k_{-1} >> k_2$ so that $k' = (k_1/k_{-1})k_2$ and the MLCT and d-d state are in equilibrium. Alternatively, $k_{-1} << k_2$ such that $k' = k_1$ and the pre-exponential term is representative of the MLCT to d-d crossover. In reported cases of ruthenium(II) complexes the first two limiting cases have been identified. For systems where $k_{-1} >> k_2$ the (A) value is typically 10^9-10^{10} s^{-1} and ΔE is *ca.* 2000 cm^{-1}. In the second case ($k_{-1} << k_2$), and as observed for $[Ru(bipy)_3]^{2+}$, ΔE is in the range 3000-4000 cm^{-1} with a pre-exponential value in the order 10^{12}-10^{14} s^{-1}.[28] It is evident that the data for (**C2**) does not fit to any of these two cases. Using the k_{obs} value at 298K of 3.8 x 10^6 s^{-1} and the quantum yield of fluorescence (ϕ_f) of 0.0092 for (**C2**), the corresponding k_r value was calculated (eq. 7) as 3.5 x 10^4 s^{-1}. For comparison the corresponding k_r value for $[Ru(bipy)_3]^{2+}$ is 7.7 x 10^4 s^{-1}.[28] Using the k_r value for (**C2**) the total non-radiative rate constant (k_{tnr}) (eq. 8) is thus 3.8 x 10^6 s^{-1}.

$$k_r = \phi_f k_{obs} \quad \textbf{Eq. 7}$$

$$k_{tnr} = k_{obs} - k_r \quad \textbf{Eq. 8}$$

3.6.2 Deactivation Model

The general deactivation model for ruthenium(II) polypyridyl complexes is best illustrated using two intersecting parabolas as shown in Figure 3.10 and in which the abscissa represents a ligand-based vibration. Since the Ru-N bond lengths in (**C2**) are very similar to analogous ruthenium(II) polypyridyl complexes it is reasonable to assume that the energy of the d-d sate is also comparable. On the other hand the luminescent MLCT state in (**C2**) is lower in energy by *ca.* 1300 cm^{-1} since its emission profile is red-shifted, and not

necessarily identical in character to the $[Ru(bipy)_3]^{2+}$ MLCT state. In general for simple ruthenium(II) bipy–based complexes k_{nr} varies linearly with emission energy such that rapid non-radiative deactivation occurs when the energy of the excited state is low. It is also known that as the energy of the MLCT decreases, the barrier ΔE gets larger so that excited state deactivation is not controlled by the thermally activated d-d state. It is evident that lowering the ^{3}MLCT potential energy surface in Figure 3.10a would result in an increase in ΔE. This conundrum however can be adequately explained if we assume that the calculated ΔE value does not correspond to the MLCT-d-d activation barrier. Since the MLCT emission band for (**C2**) is lower in energy compared to $[Ru(bipy)_3]^{2+}$, the actual ΔE value should be *ca.* 5100 cm^{-1} which affords a k' value of only 2.1 x 10^3 s^{-1}.[39] Thus, for (**C2**) the contribution to non-radiative deactivation via the d-d state is insignificant and all deactivation occurs via the MLCT state.[41] In the circumstance of (**C2**) ΔE is associated with the thermal population of another higher-lying MLCT state (Figure 3.10b), which is both consistent with the lower symmetry of the complex and the broad emission band. Overall, the general excited state behaviour of (**C2**) is consistent with a ruthenium bipy-based complex in which the appended unit does not contribute by way of a rotational mechanism to excited-state deactivation. The observed low emission from (**C2**) is consistent with efficient non-radiative deactivation as predicted by the energy-gap law.

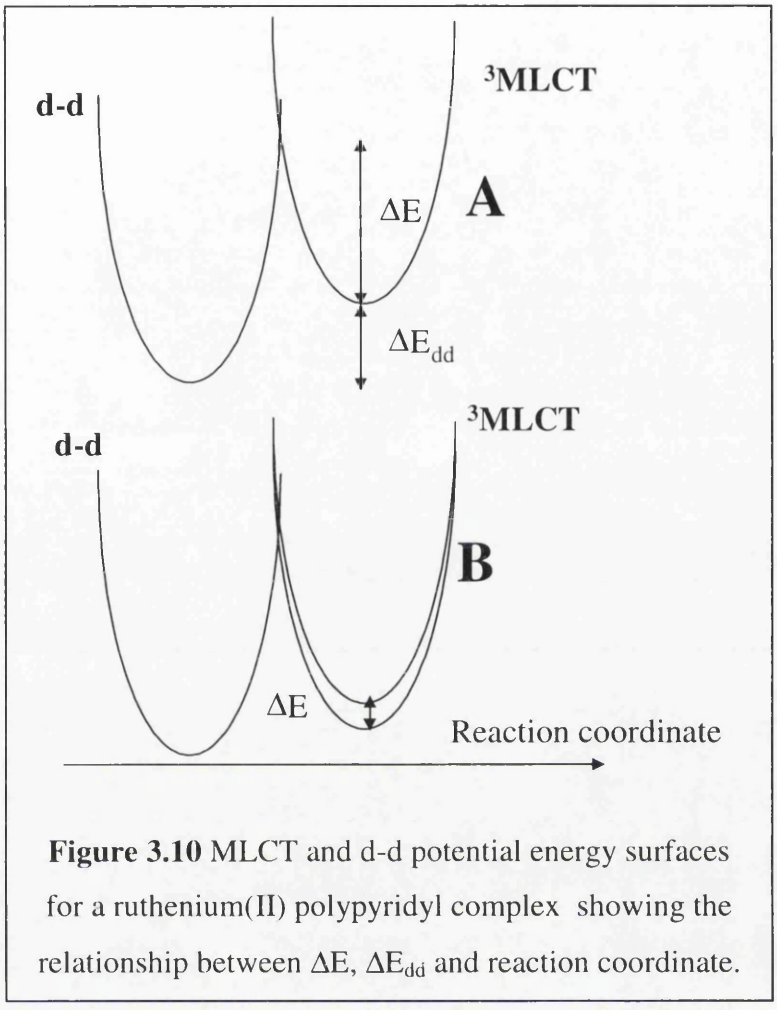

Figure 3.10 MLCT and d-d potential energy surfaces for a ruthenium(II) polypyridyl complex showing the relationship between ΔE, ΔE_{dd} and reaction coordinate.

3.7 Conclusions

The detailed photophysical study of complex (**C2**) has revealed both interesting and unexpected results. It has been found that strongly electron donating solvents can both perturb the energy of the emitting ^{3}MLCT state and the structure of the acceptor ligand. Solvent interaction is envisaged to occur at the appended *N*-methylene-4-pyridinium-4'-pyridine unit which is connected to the metal binding bipy group via a saturated methylene spacer. Perturbation of the ^{3}MLCT state is thus proposed to occur by way of a through-space dipole-dipole interaction. This result would suggest that judiciously positioned, yet

connected via saturated linkers, electron deficient groups could play a significant role in controlling the photophysical behaviour of ruthenium(II) polypyridyl complexes. Some studies using the complex **C2** for sensing have also been carried out and have given encouraging results. It has been observed that in the presence of H^+, Ni^{2+} and Cu^{2+} ions the luminescence of this complex will undergo quenching.

References

1: Balzani V., Campagna S., Denti G., Juris A., Seroni S., Venturi, M., *Acc. Chem. Res.*, **1998**, 31, 26.

2: Constable E. C., *J. Chem. Soc., Chem. Commun.*, **1997**, 1073.

3: Harriman A., Ziessel R., *J. Chem. Soc., Chem. Commun.*, **1996**, 15, 1707.

4: Burrell A. K., Gordon K. C., Simpson T. J., Waterland M. R., *J. Chem. Soc., Dalton Trans.*, **1998**, 1,185.

5: Barton J. K., Holmlin R. E., Yao J. A., *Inorg. Chem.*, **1999**, 38, 174.

6: K. Kalayansundaram, *Photochemistry of Polypyridine and Porphyrin Complexes*, 1992, Academic Press.

7: Dallinger R. F., Woodruff W. H., *J. Am. Chem. Soc.*, **1979**, 101, 4391.

8: Kavarnos G. J., *Fundamentals of Photoinduced Electron Transfer*, **1993**, VCH.

9: Beer P. D., Kocian O., Mortimer R. J., Ridgway C., *J. Chem. Soc., Faraday Trans.*, **1993**, 89, 333.

10: Armspach D., Harriman A., Matt D., *Eur. J. Inorg. Chem.*, **2000**, 6, 1147.

11: Josceanu A. M., Moore P., Sheldon P., *Rev. Roum. Chim.*, **1998**, 43, 945.

12: Alsfasser R., Geisser B., Ponce A., *Inorg. Chem.*, **1999**, 38, 2030.

13: Del Guerzo A., Demeunynck M., Lhomme J., Mesmaeker A. K-D., *J. Phys. Chem.*, **1997**, 101, 7012.

14: Barigelletti F., Flamigni L., Guardigli M., Richards C. S. W., Ward M. D., *J. Phys. Chem.*, **1996**, 100, 10620.

15: Absi M., Berg-Brennan C., Hupp J. T., Stern C., Subramanian P., *Inorg. Chem.*, **1996**, 35, 3719.

16: Benniston A. C., Harriman A., Mackie P. R., *Tetrahedron Lett.*, **1997**, 38, 3577.

17: Hau X., von Zelewsky A., *Inorg. Chem.*,**1995**, 34, 5791.

18a: Mackie P. R., *Cation Chelating [2]Catenanes and Cyclophanes based on 2,2`Bipyridine,* Phd *Thesis*, University of Glasgow, UK, 1998, pp137.

18b: Mackie P. R., *Cation Chelating [2]Catenanes and Cyclophanes base on 2,2`Bipyridine*, Phd *Thesis*, University of Glasgow, UK, 1998, pp141.

19: Benniston A. C., Mackie P. R., Yufit D. S., *Acta. Cryst. C.,* **1997,** C53, 1899.

20: Rillema D. P., Jones D. S., Levy H. A., Woods C., *Inorg. Chem.*, **1992**, 31, 2935.

21: Hush N. S., Reimers J. R., *Coord. Chem. Rev.*, **1998**, 177, 37.

22: Brunschwig B. S., Cruetz C., Sutin N., *Coord. Chem. Rev.*, **1998**, 177, 61.

23: Curtis J. C., Meyer T. J., Sullivan B. P., *Inorg. Chem.*, **1983**, 22, 224.

24: Mayer U., *Pure & Appl. Chem.*, **1979**, 51, 1697.

25: Kim H-B., Kitamura N., Obata R., Sato M., Tazuke S., *Inorg. Chem.*, **1988**, 27, 651.

26: Belser P., Balzani V., Barigelleti F., Juris A., von Zelewsky A., *Gazz. Chim. Ital.*, **1985**, 115, 723.

28: Caspar J. V., Meyer T. J., *J. Am. Chem. Soc.*, **1983**, 105,5583.

29: Kaifu Y., Koizumi M., Mataga N., *Bull. Chim. Soc. Jpn.*, **1955**, 28, 690

30: Kaifu Y., Koizumi M., Mataga N., *Bull. Chim. Soc. Jpn.*, **1956**, 29, 465.

31: Lippert E., *Z. Naturforsch*, **1955**, 10a, 541.

32: Cortés J., Heitele H., Jortner J., *J. Phys. Chem.*, **1994**, 98, 2527.

33: Kaizu Y., Matsuzawa H., Muruyama M., *Inorg. Chem.*, **1995**, 34, 3232.

34: Values of D and n taken from *Handbook of Photochemistry Vol 2* Carmichael I., Hug G. L., Murov S. L., Marcel-Dekker, 1993, pp283.

35: H-bonding solvents are excluded since these may interact with the "free" nitrogen and hence alter the electron distribution within the bipyridinium unit.

36: Calculated using $\mu_e - \mu_g = 0.010\sqrt{ma^3}$ where m = slope (cm^{-1}). Taken from ref. 30.

37: Allen G. H., Bradley P. G., Caspar J. V., Meyer T. J., Westmoreland T. D., Woodruff W. H., *J. Am. Chem. Soc.,* **1984**, 106, 3492.

38: Barquwi K. R., Meyer T. J., Murtaza Z., *J. Phys. Chem.,* **1991**, 95, 447.

39: Hupp J. T., Mines G. A., Roberts J. A., *Inorg. Chem.,* **1992**, 31, 125.

40: The new ΔE value is assumed to be 3800 cm^{-1} ($[Ru(bipy)_3]^{2+}$) + 1300 cm^{-1} (energy difference in emission energies) and A'~ 10^{14} s^{-1} .

41: This point is further supported since for a ruthenium(II) bipy–based complex with an emission energy of 14822 cm^{-1} the k_{nr} value would be *ca.* 2 x 10^6 s^{-1} (see ref. 28), which is comparable to k_{tnr} calculated for (**C2**).

CHAPTER 4

Merocyanine Derivatives

4.1 Introduction

Merocyanine dyes have been rewarded considerable interest over the years in the field of photodynamic therapy, due to their preferential uptake into leukaemia cells and the subsequent eradication of these cells.[1-3] An example of these dyes is merocyanine 540 (figure 4.1).

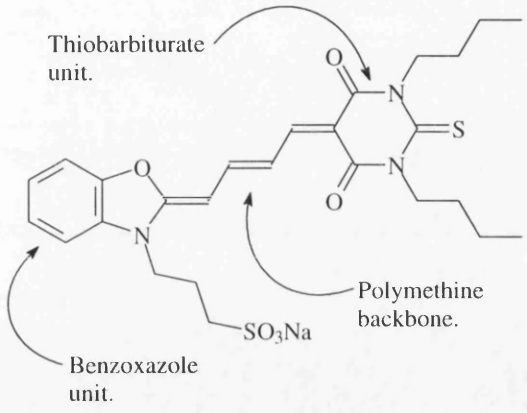

Figure 4.1. Merocyanine 540

There are three main structural units within these dyes they are, the benzoxazole unit, polymethine backbone and the thiobarbiturate unit. From full structural analysis, it has been established that the polymethine backbone has the all-trans conformation in the ground state. When in this conformation an intramolecular hydrogen bond exists between the polymethine backbone and one of the carbonyl groups on the

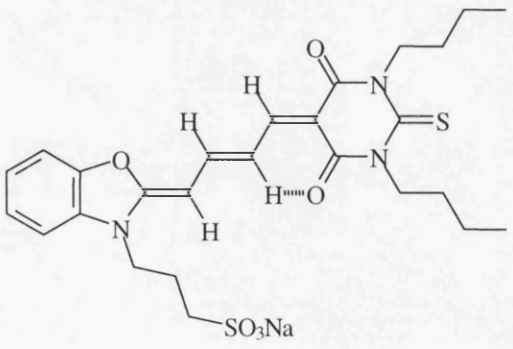

Figure 4.2. Intramolecular H-bonding within merocyanine dyes.

thiobarbiturate unit (figure 4.2), this has been confirmed from FTIR spectra.[4]

It has also been shown that these dyes may exist as several zwitterionic forms resulting from the internal electronics of these molecules (scheme 4.1). The major contributing factor to the formation of these forms is that of the N-atom of the aromatic region (benzoxazole unit) acts as the primary electron donor and the carbonyl groups on the thiobarbiturate sub-unit acts as the main electron acceptors. As a result of this it has been found that these dyes are quite polar, having dipole moments of *ca.* 10 D.

This polarity is not only attributed to the presence of the zwitterionic forms but is also a result of the overall spread of electrons within the molecule. In particular the C-N amide bonds can possess partial double-bond characteristics resulting in the extension of the conjugation throughout the entire molecule.

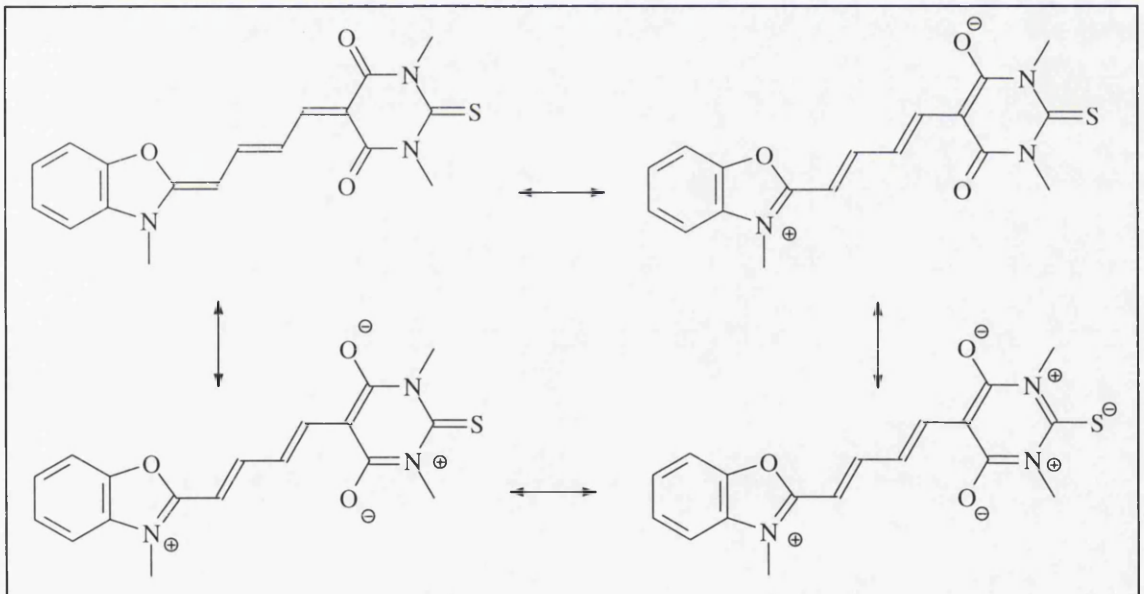

Scheme 4.1. Zwitterionic forms of merocyanine dyes

4.2 Photophysical properties of merocyanine dyes

A number of research groups have reported on the photochemical properties of merocyanine dyes in fluid solutions and in microheterogeneous media.[5-11] Merocyanine dyes have two photophysical properties that can be employed in sensing and photodynamic therapy, intense fluorescence and intersystem crossing to the triplet manifold. Firstly, the intense florescence contributes to their use as a diagnostic tool and secondly intersystem crossing as a photosensitizer. When this intersystem crossing takes place in the presence of molecular oxygen the result is the formation of singlet oxygen. This production of singlet oxygen will lead to the death of the infected cells. Unfortunately the efficiency of these two processes is greatly diminished due to the presence of a third process the dominant photoprocess of these dyes.

This process involves the photo-isomerization of the polymethine backbone to form a long-lived (unstable) cis-isomer. This isomerization process is believed to be attributed to an electronically excited singlet state (S_2), which possesses a twisted geometry.[12] This excited state would then under go internal conversion to form the cis-isomer (figure 4.3).

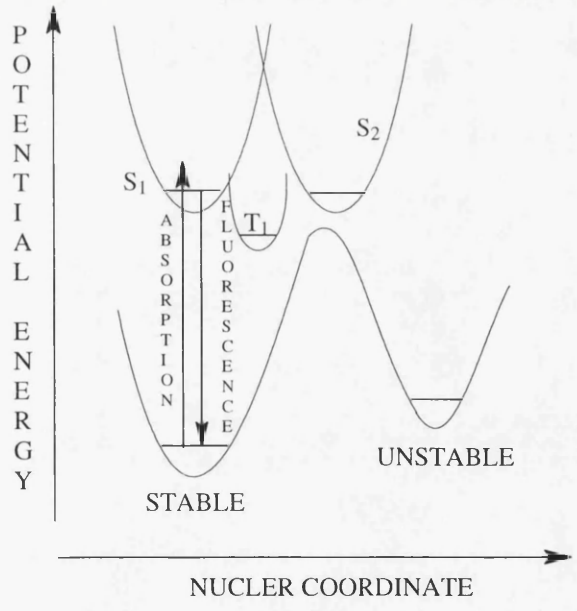

Figure 4.3 Simplified potential energy diagram for the isomerization of merocyanine dyes.

From laser flash photolysis carried out in N_2-saturated conditions both the isomer and the triplet can be seen in the differential absorption spectra with peaks at 595nm and 660nm. When this experiment was repeated in aerated conditions only one of these peaks remained, the peak at 595nm and was attributed to the long-lived cis-isomer, as the short lived triplet would have been quenched by molecular oxygen. The peak at 660nm was therefore assigned to the triplet.

It is believed that if the isomerization process could be prevented or inhibited the outcome would be that of a considerably improved photosensitizer or sensor, as formation of the isomer would not occur and production of the triplet and/ or fluorescence would be enhanced.

4.3 Prior studies into the prevention of the isomerization

Prior studies into the prevention of this isomerization process carried out mainly by Benniston and Harriman have unfortunately failed to produce derivatives that were substantially better than the parent dye merocyanine 540.[4,13-16] These studies involved structural and electronic changes within the molecule and are outlined in the following pages.

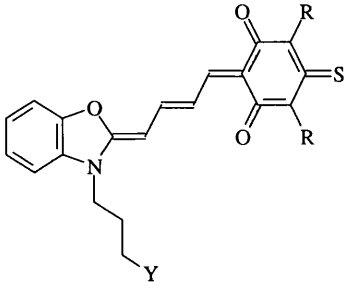

Figure 4.4 Lengthening of the of side chains R and Y.

Structural changes.

The first strategy adopted was lengthening of the chains attached to the benzoxazole and thiobarbiturate unit as isomerization would involve the rotation of one of these groups (figure 4.4). The results of this study found that the isomerization process involved the rotation of the

benzoxazole unit via the isomerization of either the first or second double bound in the backbone. The third double bond should not be involved as it is locked into the trans conformation through the intramolecular H-bond.

As for the effect on the photophysical properties it was found that the lengthening of these chains had very little effect on the fluorescence and intersystem crossing. So these processes must occur independently to the nature of these chains. However it was found that as the length of the Y group increased there was a slight effect on the rate of isomerization. From this it was concluded that as the volume of the rotor group increased the rate of isomerization decreased. In other words as the size of the group rotating became larger the harder the molecule found it to undergo isomerization.

The next step towards attempting to understand the isomerization process was to constrain or hinder the isomerization of the second double bound in the backbone as it was thought to be the most likely responsible for the isomerization process. This was attempted by incorporating it into a ring structure or by the addition of bulky groups onto the polymethine backbone (figure 4.5).

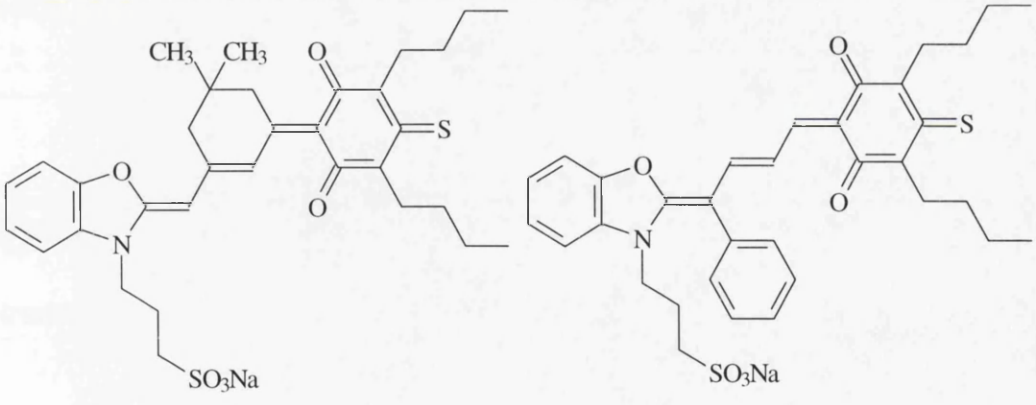

Figure 4.5 Addition of bulky groups to the backbone to hinder isomerization.

This was expected to prevent isomerization in two ways:-

1. Sterically by hindering the rotation of the double bound via the shear size of the groups and by an increase in the volume of the rotor group.
2. Electronically by lowering the effect of the zwitterionic forms have on the isomerization process by perturbing the bond angle between the N-C-C bonds.

These change in the molecule were found to increase the bond order of the central double bond, therefore this bond should have greater rigidity and not under go isomerization as readily as the parent dye.

However these derivatives failed to produce molecules that gave better fluorescence or intersystem crossing than the parent dye merocyanine 540. Nevertheless these derivatives did give insight into the isomerization process. It was found from these studies that even though there was not an increase in the favourable photo-processes, the rate of isomerization also decreased. However, an increase in the rate of internal conversion occurred. It was concluded that this internal conversion occurs at the first double bound resulting in a perpendicular transition state between the two isomers (figure 4.6), from this information it was suspected that the isomerization process occurs at the first double bound.

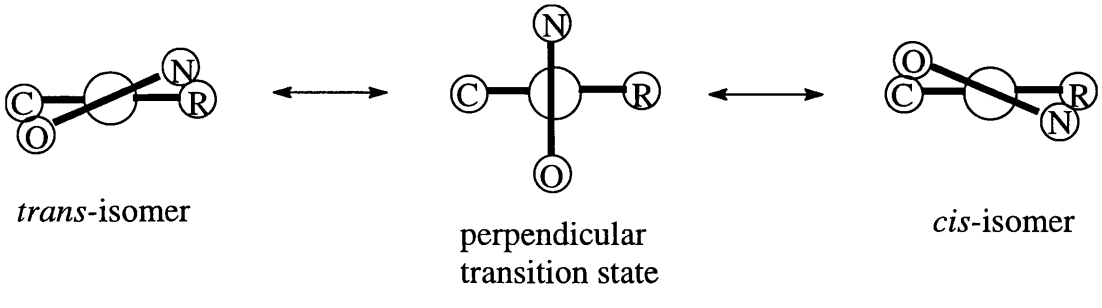

Figure 4.6 Formation of the perpendicular transition state.

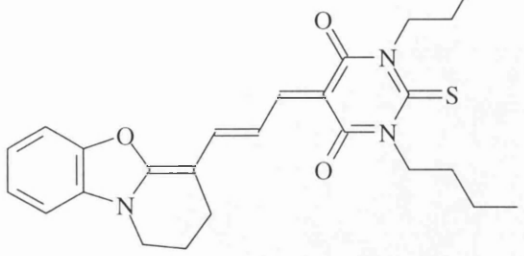

Figure 4.7 Constraining the first double bound.

The final strategy attempted to prevent the isomerization via structural changes, was that of constraining the first double bound of the backbone. This was thought to be the structural change that would finally prevent isomerization, producing a viable dye that could be used in photodynamic therapy (figure 4.7).

The results of this study however were to prove other wise. It was found that this derivative was different to MC540 in the following ways: -

1. The dye was less fluorescent.
2. Photoisomerization still took place despite the constraining group.
3. The triplet state was formed but in low yield.

The lower fluorescence and low formation of the triplet-state was determined to be caused by structural distortion as a result of adding the constraining propyl chain. This in turn perturbed the absorption spectrum and decreased the rate of radiative decay. As for photoisomerization it was found that when the first double bound was constrained, the second double bond undergoes rotation to give rise to the cis-isomer.

From this information it is unclear which of the two double bonds the isomerization process take place at in the parent dye MC540.

Electronic Changes.

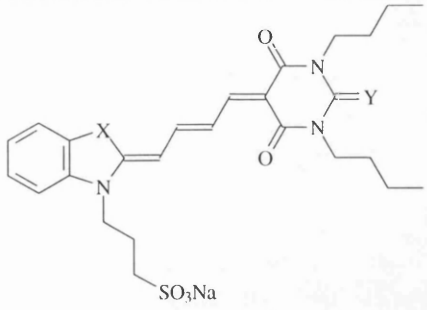

Figure 4.8 Changing of the hetero atoms present in the dye.

This strategy was based on the presence of the zwitterionic forms of the dye described earlier in this chapter. The result of the formation of these zwitterions is the lowering of the bond order of the suspected bonds that under go isomerization. It was therefore thought that by changing the heteroatoms X and Y the overall polarity of the system would be perturbed enough to prevent the formation of zwitterionic forms (figure 4.8). In turn raising the bond order of the double bonds in the backbone and prevent isomerization.

It was found that on changing the Y atom to an oxygen atom the overall dipole moment of the molecule increased. This was a result of a stabilising effect caused by the oxygen, increasing the conjugation of the end group and increasing its ability to accept electrons. This is possible as the electronic charge can now be spread over the three oxygens in the end group. This effect can be seen in the results of the photophysical studies carried out on this derivative. It was shown that the molecule had an increased rate of photoisomerization and internal conversion and a decrease in the formation of the triplet in comparison to the parent dye MC540. However it was also found that the fluorescence of this derivative increased. Other results discovered by changing the heteroatoms showed that on changing the Y atom to a selenium atom the rate of uptake into infected cells of the dye may be increased. Also if the X atom is also changed to a selenium atom the triplet yield may be increased making them much more potent photosensitizer, but unfortunately the isomerization process still occurs.

4.4 Aim and derivative design

The overall aim of this project is the design and synthesis of merocyanine derivatives that will not undergo photoisomerization when illuminated, in the hope of enhancing the other photo properties that these dyes possess. With the improvement of these properties their use in photodynamic therapy and their ability to act as optical sensors should increase drastically. Two derivatives **MC1** (figure 4.9) and **MC2** (figure 4.10) were designed in order to accomplish this.

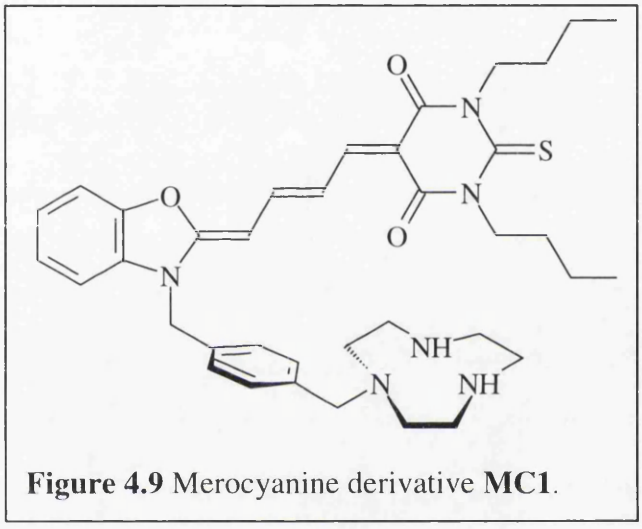

Figure 4.9 Merocyanine derivative **MC1**.

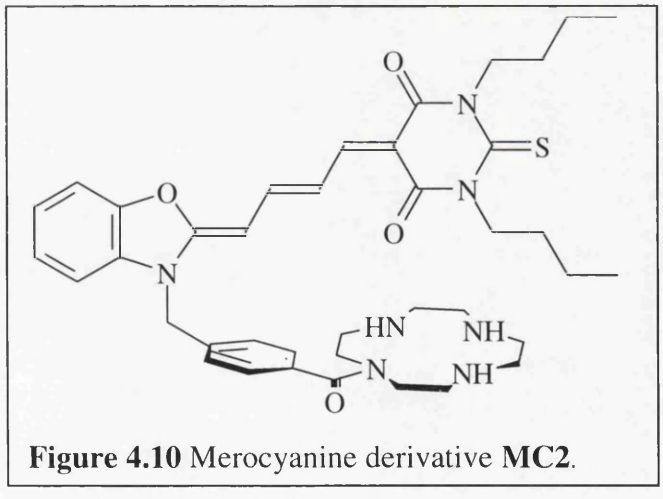

Figure 4.10 Merocyanine derivative **MC2**.

4.4.1 Use of a binding site (sterically)

In both the derivatives above a macrocyclic binding site has been incorporated into the structure of the molecule. By the incorporation of a macrocycle in this way it is believed that the isomerization process will be prevented, by locking the structure into the trans isomer. From molecular modelling studies it can be shown that the binding sites are in good orientation that when bound to a metal, one of the carboxylate groups present on the thiobarbiturate unit will also be bound. This binding of the carboxylate should in turn prevent the isomerization process from occurring, as the backbone will be unable to rotate.

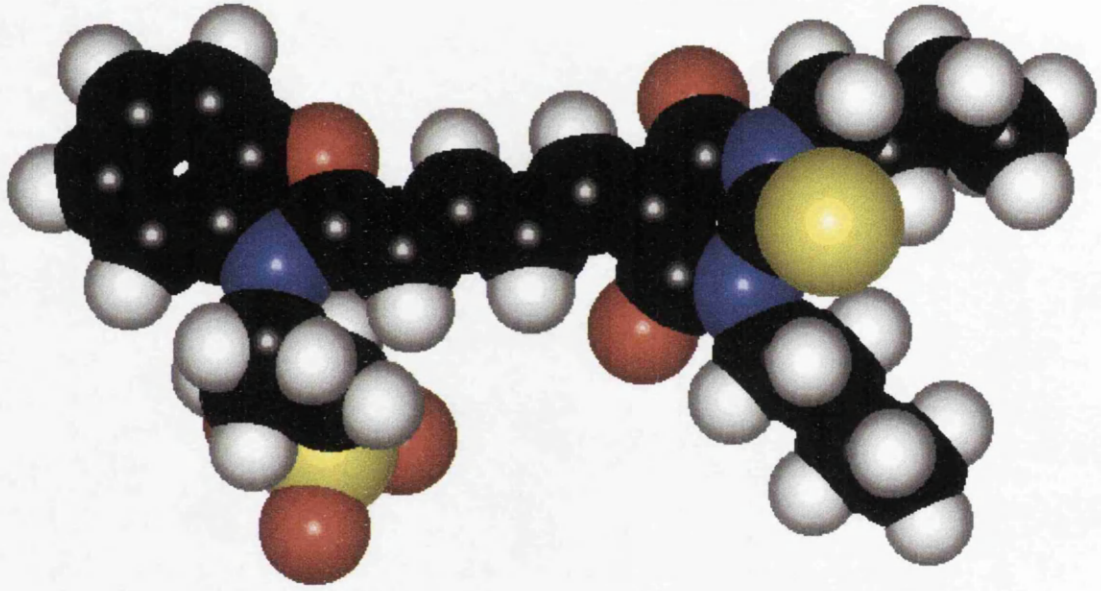

Figure 4.11 MM+ space filled model of MC540. Black=carbon, White=hydrogen, Red=oxygen, Blue=nitrogen, Yellow=sulphur.

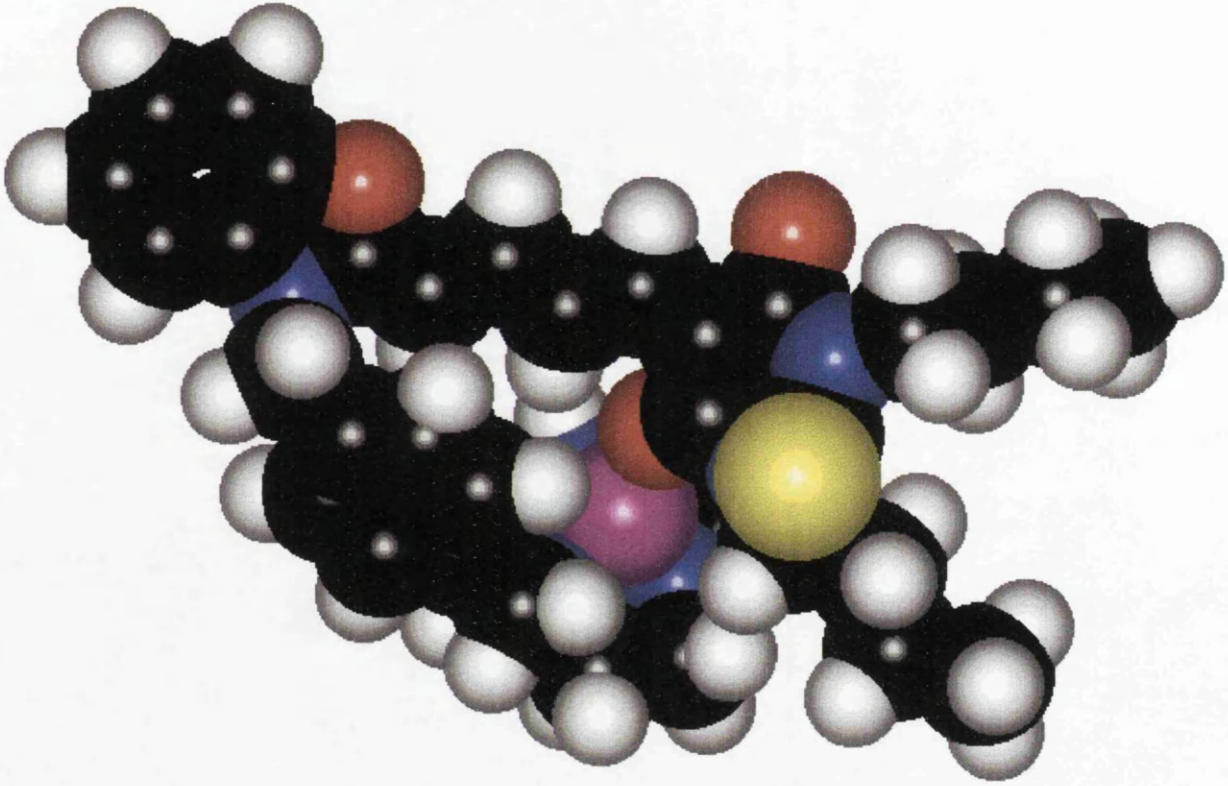

Figure 4.12 MM+ space filled model of MC1 Black=carbon, White=hydrogen, Red=oxygen, Blue=nitrogen, Yellow=sulphur, Purple=zinc.

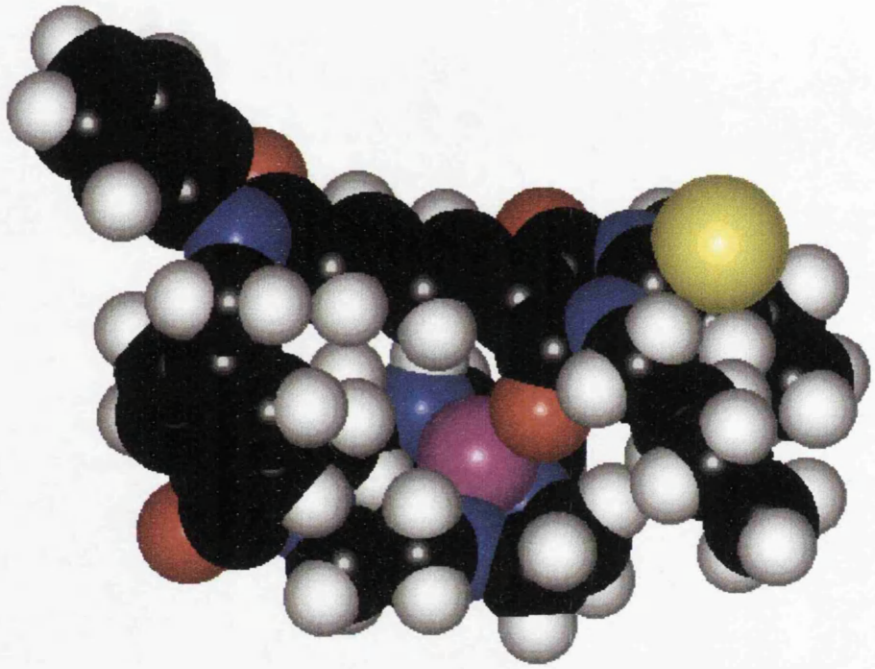

Figure 4.13 MM+ space filled model of MC2 Black=carbon, White=hydrogen, Red=oxygen, Blue=nitrogen, Yellow=sulphur. Purple=Zinc

4.4.2 Use of a binding site (electronically)

As well as constraining the entire backbone into its trans configuration it is believed that an electronic effect will also aid in the prevention of the isomerization process. Although this binding process may not prevent the formation of the zwitterionic forms of the dye, the formation should in turn strengthen the bond between the carboxylate and the metal (figure 4.14). So even though the zwitterionic forms are present it should have very little effect on the isomerization process.

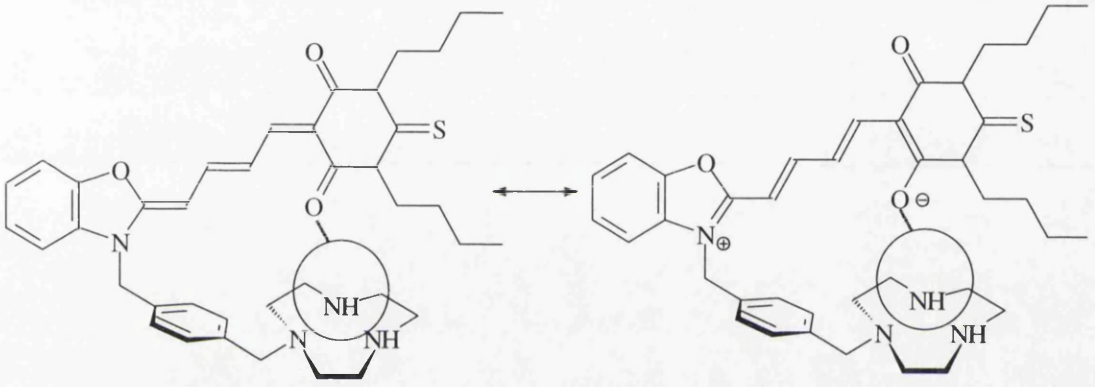

Figure 4.14 Proposed effect of metal binding on the zwitterionic form.

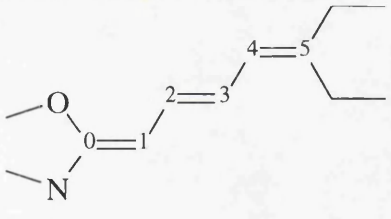

Figure 4.15 Numbering of the carbons on the backbone.

From molecular modelling it is possible to investigate further into the effects this binding has on the backbone of the derivatives in comparison to merocyanine 540. From the models the bond lengths and the bond orders of the bonds within the backbone were calculated and are shown in table 4.1.Numbering of the carbons in the backbone is shown in figure 4.15.

	MC 540		MC 1		MC 2	
	Bond length Å	**Bond order**	**Bond length Å**	**Bond order**	**Bond length Å**	**Bond order**
$C_0=C_1$	1.344	1.695	1.341	1.711	1.345	1.687
C_1-C_2	1.345	1.686	1.344	1.693	1.471	1.115
$C_2=C_3$	1.347	1.676	1.347	1.676	1.346	1.682
C_3-C_4	1.347	1.676	1.345	1.686	1.472	1.111
$C_4=C_5$	1.351	1.654	1.352	1.649	1.347	1.676

Table 4.1 Bond lengths and orders of the bonds in the polymethine backbone calculated with MM+.

It can be seen from the results of these calculations that the derivative **MC1** in comparison to **MC540** has double bonds which remain at almost the same bond order, but the bond order of the single bonds rise slightly. This could be a result of the zwitterionic form of the dyes being stabilized by the binding site. The overall effect of this increase in bond order is a more rigid molecule, which would imply that the molecule would be less likely to undergo isomerization.

As for the second derivative **MC2** it can be seen that the opposite happens the bond order of the double bonds increase slightly and the bond order of the single bonds are drastically reduced. This would suggest that for this derivative the formation of the zwitterionic form would be unfavourable and would prevent isomerization. However this effect should have very little contribution to whether isomerization occurs or not as the

major contribution to preventing isomerization will be that of the molecule being locked by the binding of carbonyl to the metal.

4.4.3 Supporting evidence

A report by Inouye *et al.* has shown that by incorporating a crown ether into spirobenzopyrans that the subsequent binding of an alkali metal to these molecules may induce it to isomerize to their merocyanine form (figure 4.16).[17]

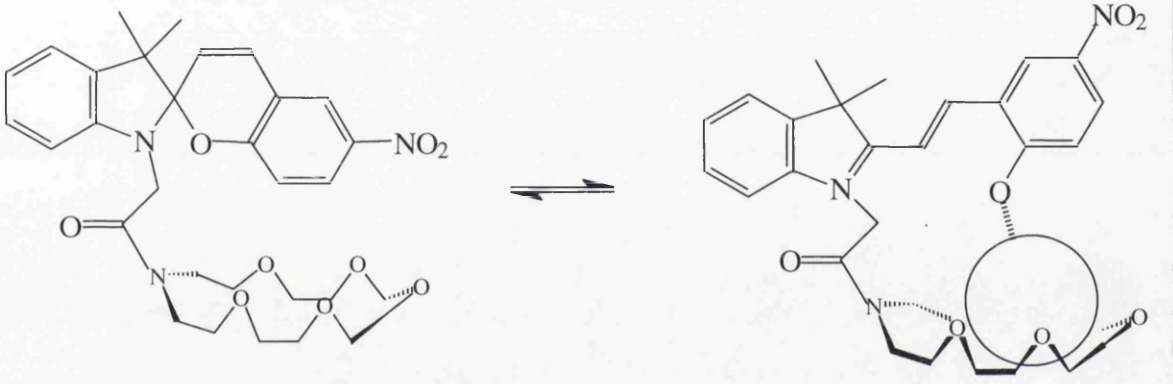

Figure 4.16 Induction of the isomerization of spirobenzopyrans on binding a metal.

4.5 Derivatives as sensors

The binding of metals to **MC1** and **MC2** could be monitored in two ways. Firstly, the fluorescence of these molecules should be effected, as the photoisomerization process will be prevented to give increased fluorescence. Secondly, from laser flash photolysis the differential absorption spectra should be different, as the cis-isomer will not be formed. This can be monitored, as the peak of the cis-isomer at around 595nm in the absorption spectra should not be present. Therefore these dyes could be used to sense for metals by monitoring changes in these spectra.

4.6 Preliminary consideration for synthesis

The macrocycles used in these derivatives are aza-macrocycles and a problem arises from using these types of macrocycles. This is due to the reactivity of the nitrogens within the rings, which results in a difficulty to mono-alkylate the ring.

For **MC1** the macrocycle used is tacn and the problem of mono- alkylation can be overcome for this particular macrocycle by capping it. This capping process is carried out by heating the tacn with N,N-dimethylformamide-dimethylacetal under nitrogen to produce 1,4,7-triaazatricyclo[5.2.1.0]decane.[18] This capped tacn can then be efficiently mono-alkylated using an alkyl bromide to give the quaternary amine salt.[19] The mono-alkylated tacn can then be obtained from base hydrolysis to give the required product (figure 4.17).

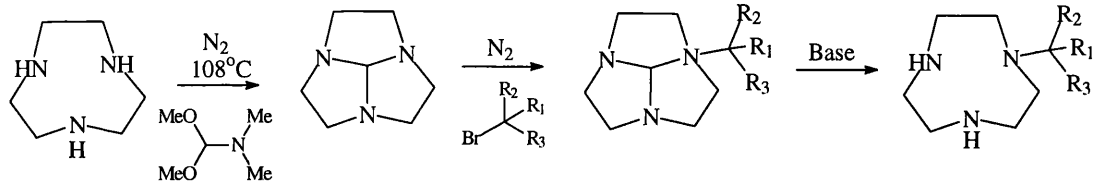

Figure 4.17 Mono alkylation of tacn.

The mono-alkylation of **MC2** may prove to be a little trickier as it is not tacn that is used as the macrocycle. In this case it may be necessary to carry out the alkylating process under high dilution conditions in order to obtain the product.

4.7 Reaction schemes

4.7.1 Synthesis of MC1

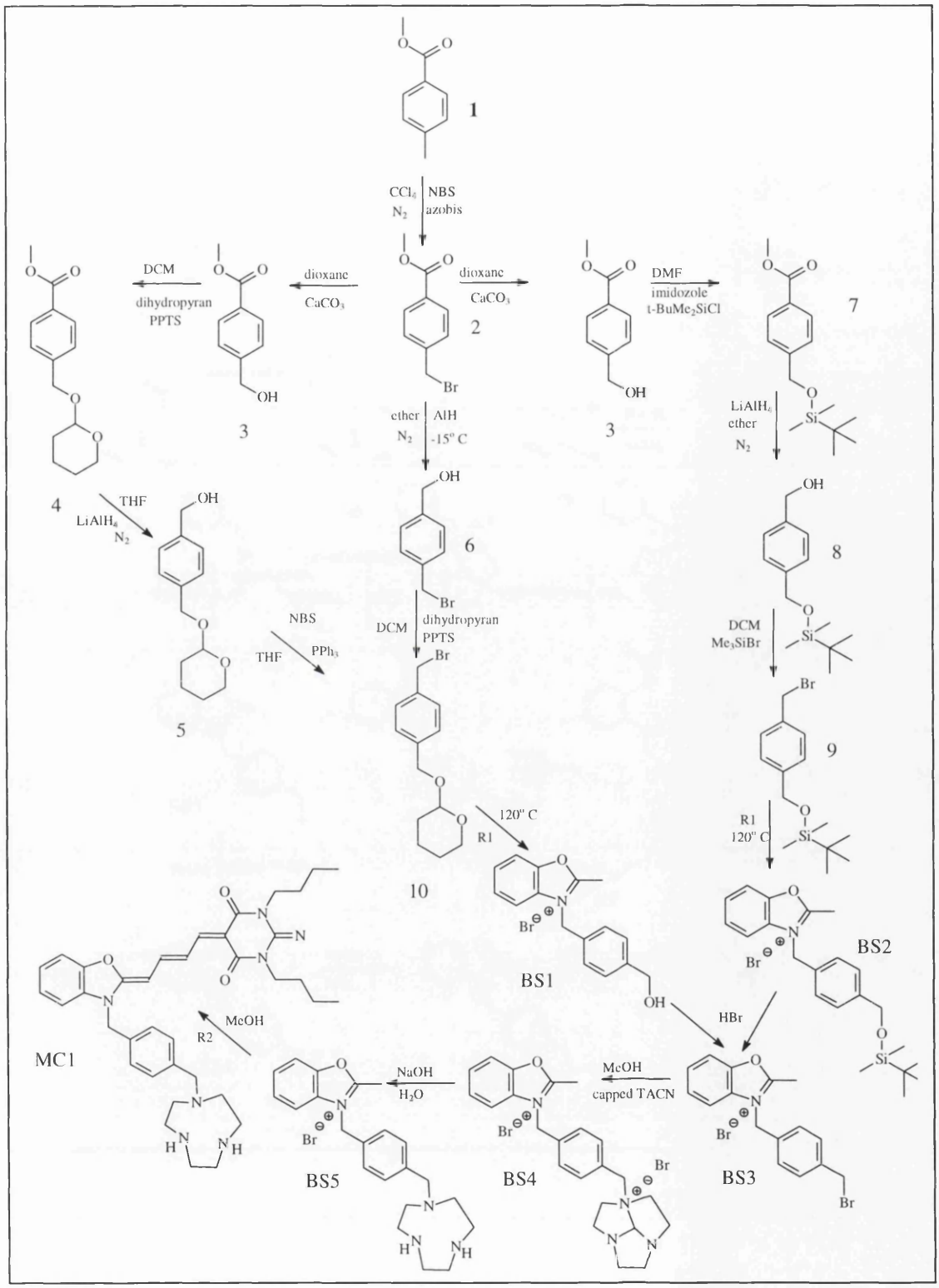

4.7.2 Synthesis of MC1 scheme 2

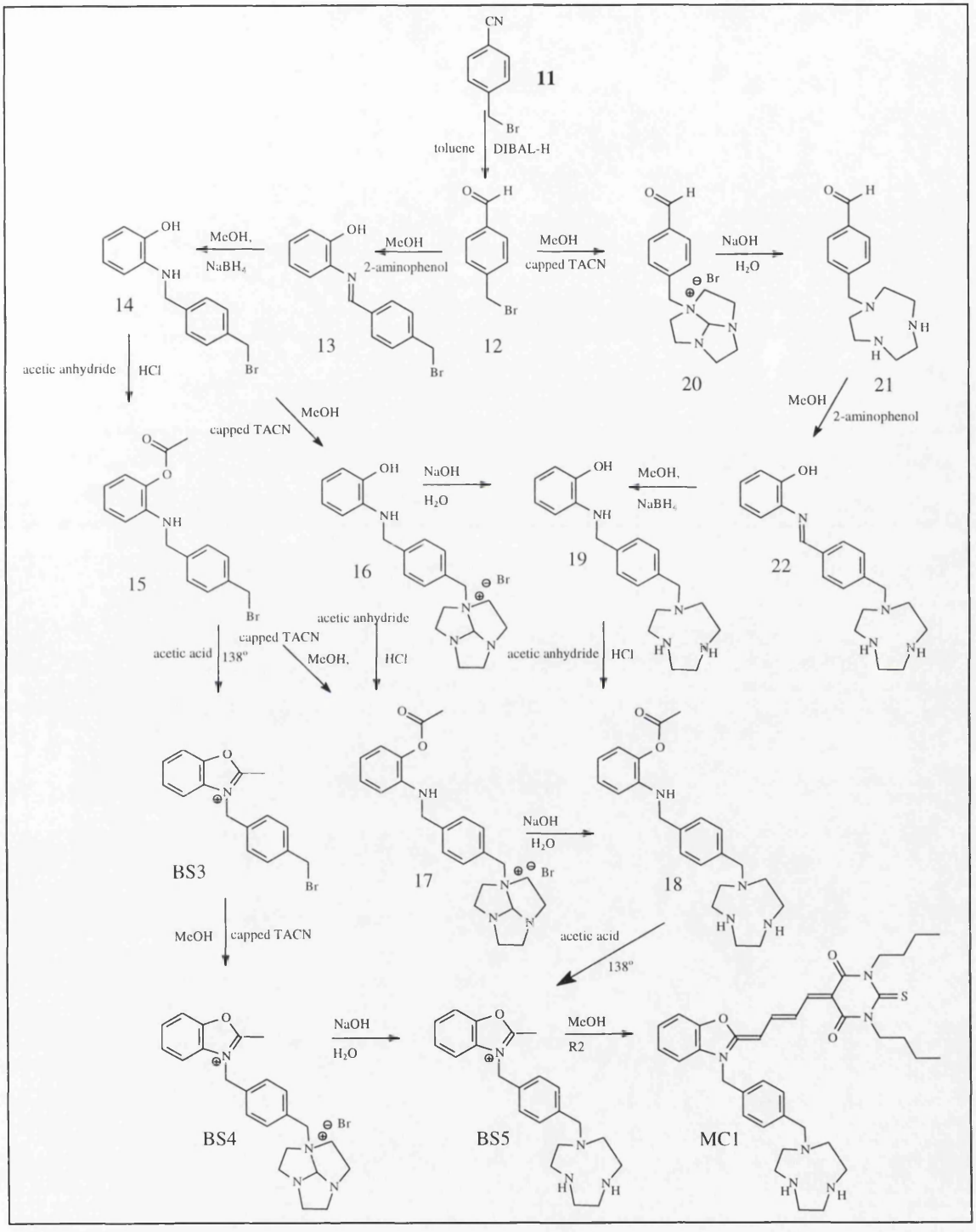

4.7.3 Synthesis of MC2 scheme 3

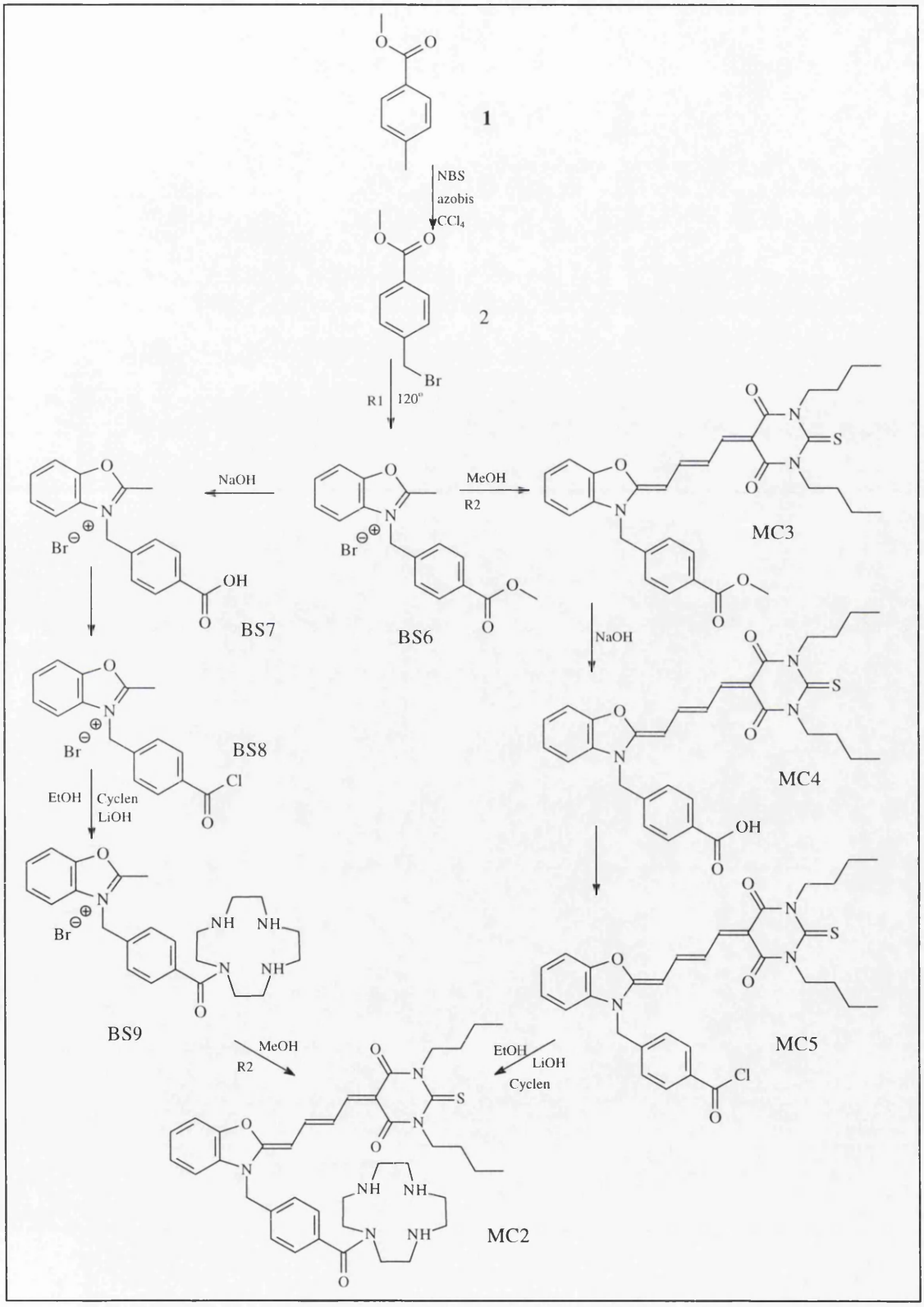

4.8 Discussion of synthesis

4.8.1 General consideration

Throughout the reaction schemes there are various point at which the macrocycle can possibly be attached to the compound. In the case of **MC1** the attachment of the macrocycle will involve the removal of the cap required for the mono functionalization of the tacn, and will involve the use of base. It is believed that this process should be carried out before the generation of the dye, as the polymethine backbone is very susceptible to base and will readily degenerate and result in the destruction of the dye. Consequently it would be preferable if the entire benzoxazole unit with the uncapped tacn attached was fully synthesized before the preparation of the dye.

4.8.2 Reaction scheme 1

At first synthesis of **MC1** was attempted via the outer routes of reaction scheme 1 and involved the bromination of a hydroxide group, within a compound containing another hydroxide group protected with either a pyran (**5**) or silyl ether (**8**) group. This bromination step was found to be tricky and several attempts were made without success. Firstly the silyl ether group was reacted with trimethylsilylbromide but this resulted in the formation of a white solid that was determined to be the di-bromide species. This is thought to have occurred due to the formation of an intermediate that contains a leaving group possessing a very similar rate constant as the protecting group for the substitution with bromide figure 4.18.

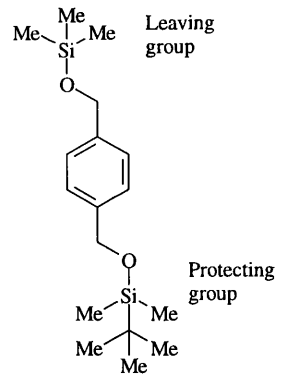

Figure 4.18 Proposed intermediate.

Secondly the pyran-protected compound was reacted with n-bromosuccinimide and triphenylphosphine after the reaction and work up a yellow oil was isolated. It was found that there had been no reaction as the NMR of the product was the same as the starting material.

The final attempt was carried out on both the silyl and the pyran protected compounds and involved the reagent phosphorous tri bromide and resulted in the formation of the di-bromide species.

At this point synthesis of **MC1** was attempted via the middle route of reaction scheme 1. This route involves compound **6** a very unstable molecule that will decompose at high temperatures making the reaction of **6** with benzoxazole impossible, as it is a melt reaction carried out at 120° C. Protecting the alcohol group with dihydropyran giving **10** easily solved this problem and successfully gave a stable product that could be used in the melt reaction.

The next problem to be encountered was in the next step the synthesis of **BS1**. The melt reaction of **10** and benzoxazole should have given a product which when triturated with diethyl ether would give a white salt. Instead the brown sticky product gave a brown salt after triturating with ether, the salt rapidly reacted with water vapour in the atmosphere to revert back to a brown sticky mass. The NMR of this compound showed it was the desired product but impure. Attempts to purify the product failed and are outlined below:

1. Recrystallization.

The product was found to be very insoluble in many solvents except for methanol and ethanol. So the product was dissolved in ethanol and attempts to precipitate it with a solvent of lower polarity only resulted in brown impure salts.

2.Conversion of the counter ion to PF_6.

It was then thought that by converting the bromide counter ion to hexafluorophosphate would be a viable way of purifying the salt. This was attempted by dissolving the salt in water and adding ammonium hexaflorophosphate to precipitate it as the pure product. This strategy also failed as it was found that the product was sparingly soluble in water.

3. Chromatography.

A silica column was then tried but did not give adequate separation. Ion exchange columns were then considered but dismissed as the product was sparingly soluble in water.

A final attempt to synthesise compound **BS1** was then tried using a high boiling point solvent to dissolve the reactants and then to reflux them at 120° C in the hope that the product would precipitate out as it was formed. This however also failed as no reaction occurred. At this point reaction scheme 1 was abandoned due to the inability to purify **BS1**.

4.8.3 Reaction scheme 2

An alternative reaction scheme was then devised for the synthesis of **MC1**, as shown in reaction scheme 2 the basis of this strategy was to avoid working with benzoxazolium salts, which were the main problem encountered in reaction scheme 1.

Synthesis of **MC1** via scheme 2 should be a cleaner and easier method as the benzoxazolium salt is prepared via a ring closure reaction instead of a harsh melt reaction.

This is expected as the salt generated will precipitate out of the reaction medium as it is formed which would be beneficial as the product could be filtered and used in the next step of reaction scheme 2. The current point of preparative work for reaction scheme 2 is **20** and **14**.

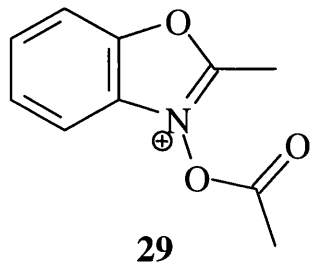

29

Figure 4.19 Benzoxazolium salt BS10.

While this work was been carried out a paper by Takeuchi and Koyama[10] was found that highlighted a possible problem that could be encountered with the ring closure step. The ring closure step in scheme 2 is possible by heating **15** or **18** in acetic acid at 138°C. However the problem highlighted in this paper is that the thermal reaction of 2-acetamidophenyl acetate with acetic acid forms 2-methyl benzoxazole via the expulsion of the acetate group, instead of forming the benzoxazolium salt **BS10** (figure 4.19).

4.8.4 REACTION SCHEME 3

A tetraazamacrocycle was chosen for **MC2** instead of a triaza, as the nitrogen in the amide group will not contribute to the binding of a metal.

It was found that when compound **2** was used in the melt reaction with benzoxazole a much cleaner reaction took place and gave rise to **BS6**, which was easily triturated with ether to give a pure product. **BS6** was then successfully reacted with the thio-barbiturate backbone unit and purified to give **MC3** and is the current point of preparative work for reaction scheme 3. From this a COSY NMR spectra was obtained and allowed for the complete assignment of the peaks to the structure as shown in figure 4.20.

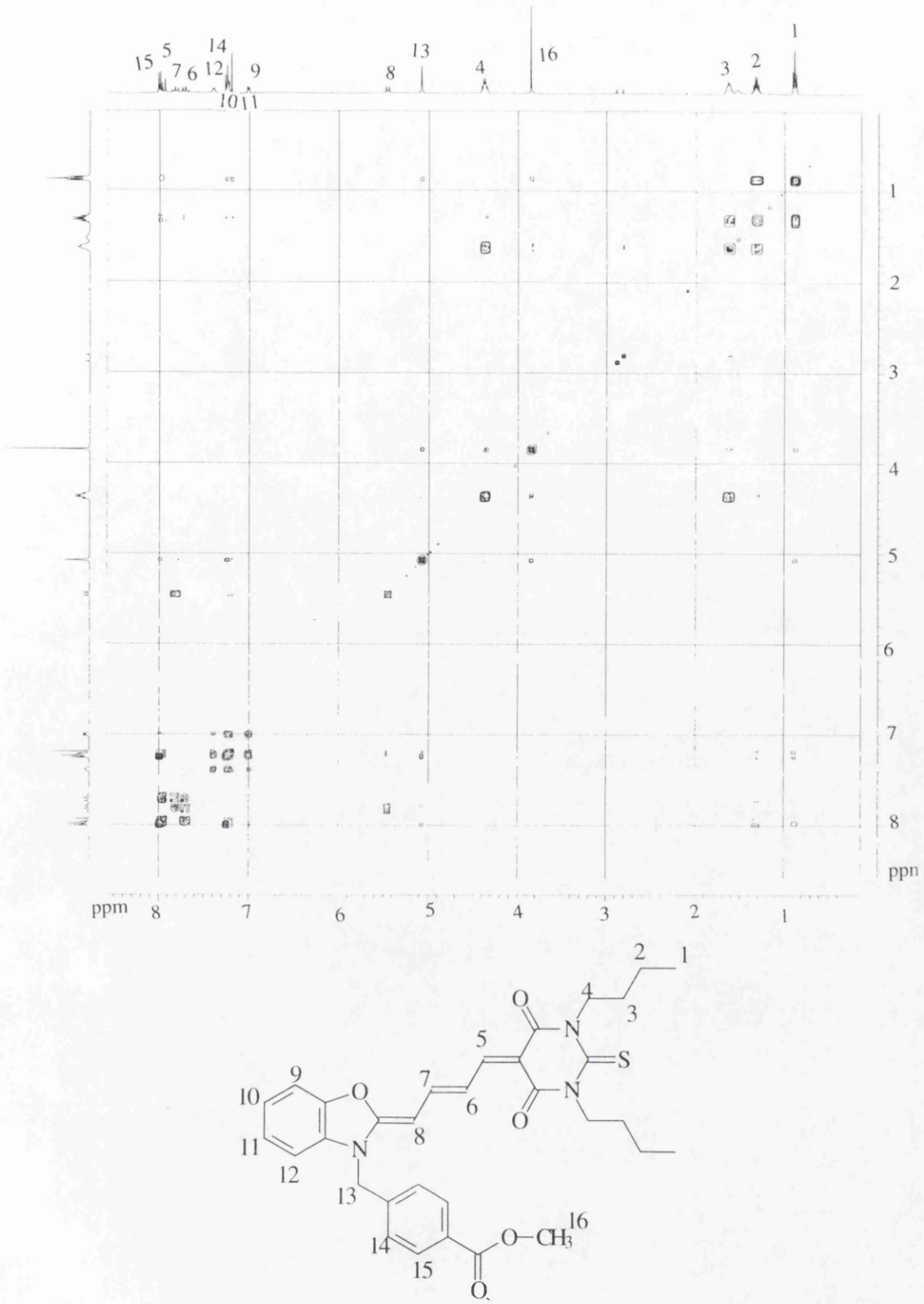

Figure 4.20 The 400MHz two-dimensional COSY NMR spectrum for **MC3** in $CDCl_3$ and the assignment of peaks.

The next step in scheme 3 is the hydrolysis of the ester group. It is essential that this step be carried out under very mild reaction conditions, as the polymethine backbone is very susceptible to acid and base conditions. After this step has been successfully carried out there are two options open for consideration: -

1. Attempt to attach the macrocycle.
2 Determine whether or not the carboxylic acid group can be used to bind metals in order to prevent the isomerization within the molecule.

4.9 Conclusions

As yet the target molecules **MC1** or **MC2** have been synthesized. **MC1** encountered problems during reaction scheme 1 in particular the purification of **BS1**, and so the synthesis of **MC1** was subsequently abandoned by this route. An alternative reaction schemes for the synthesis of **MC1** has been devised and at present seems to give a viable route towards the synthesis of **MC1**. Synthesis towards **MC2** has been relatively successful allowing for the synthesis of **MC3.**

References

1: Gomer C. J., *Photochem. Photobiol.*, **1991**, 54, 1093.

2: Sieber F., *Photochem. Photobiol.*, **1987**, 46,1035.

3: Harriman A., Neta P., Shoute L. C. T., *J. Phys. Chem.*, **1991**, 95, 2415.

4: Benniston A.C., Gulliya K. S., Harriman A., *J. Chem. Soc. Faraday Trans.*, **1994**, 90 (7), 953.

5: Filix J. B., Girotti A. W., Kalyanaraman B., Sieber F., Thomas J. P., *Proc. Natl. Acad. Sci. USA*, **1987**, 84, 2999.

6: Davila J., Gulliya K. S., Harriman A., *Photochem. Photobiol.*, **1991**, 53, 1.

7: Hoebeke M., Piette J., Van der Vorst A., *Photochem. Photobiol. B: Biol.*, **1991**, 9, 281.

8: Davila J., Gulliya K. S., Harriman A., *J. Chem. Soc., Chem. Commun.*, **1989**, 1215.

9: Aramendia P. H., Bittersmann E., Braslavasky S. E., Nitsch C., Krieg M., *Photochem. Photobiol.*, **1988,** 48, 187.

10: Dixit N. S., MacKay R. A., *J. Am. Chem. Soc.*, **1983,** 105, 2928.

11:Filix J. B., Girotti A. W., Kalyanaraman B., Pintar T. J., Singh R. J., *Photochem. Photobiol.*, **1991**, 53, 345.

12: Harriman A., *J. Photochem. Photobiol. A*, **1992**, 65, 79.

13: Benniston A.C., Gulliya K. S., Harriman A., *J. Chem. Soc. Faraday Trans.*, **1997**, 93 (15), 2491.

14: Benniston A.C., Harriman A., McAvoy C., *J. Chem. Soc. Faraday Trans.*, **1997**, 93 (20), 3653.

15: Benniston A.C., Harriman A., McAvoy C., *J. Chem. Soc. Faraday Trans.*, **1998**, 94 (4), 519.

16: Benniston A.C., Harriman A., *J. Chem. Soc. Faraday Trans.*, **1998**, 94 (13), 1841.

17: Akamatsu K., Inouye M., Nakazumi H., *J. Am. Chem. Soc.*, **1997**, 119, 9160.

18: Atkins T. J., *J. Am. Chem. Soc.*, **1980**, 102, 6364.

19: Gronbeck D. G., Johnson van B., Vachon D. J., Weisman G. R., *J. Chem. Soc., Chem. Commun.*, **1987**, 886.